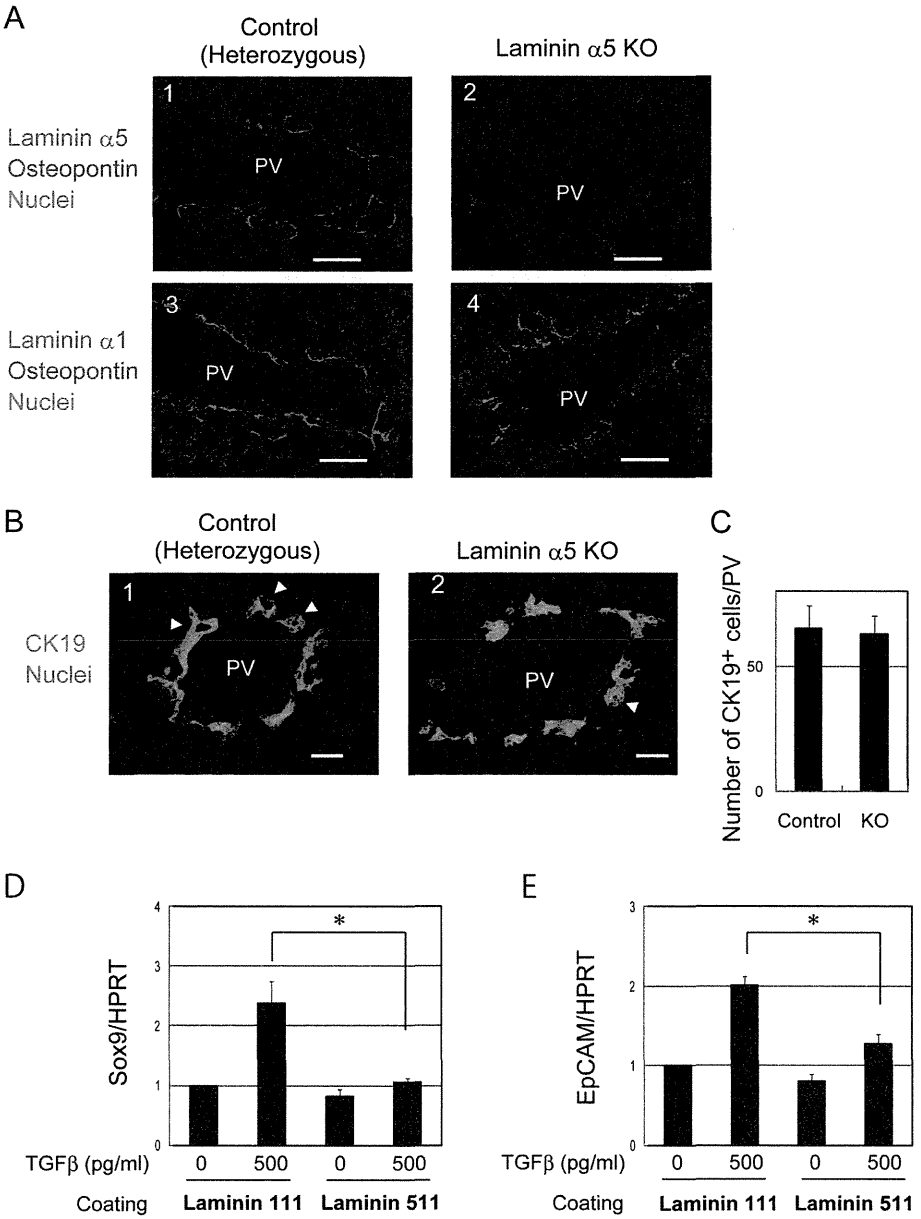

FIGURE 5. **Laminin α5 is dispensable for the lineage determination of hepatoblasts to cholangiocytes.** *A*, laminin α5 is not observed at the basal side of cholangiocytes in laminin α5 KO livers, whereas laminin α1 is normally expressed. The control and laminin α5 KO livers were stained with anti-laminin α5 (*panels 1* and *2*) or anti-laminin α1 (*panels 3* and *4*) and anti-osteopontin antibodies. *Bars* represent 50 μm. *B*, CK19$^+$ cholangiocytes are observed around the portal vein in laminin α5 KO liver. E17.5 liver sections were stained with anti-CK19 antibody. *Arrowheads* indicate luminal structures surrounded by CK19$^+$ cells. *C*, numbers of CK19$^+$ cholangiocytes in the control and mutant livers. The number of CK19$^+$ cholangiocytes around the portal vein was counted in liver sections prepared from two control and three mutant livers. There was no statistically significant difference between the control and KO. A *t* test was performed by Microsoft Excel software. *D* and *E*, TGFβ induces Sox9 and EpCAM, cholangiocyte markers, in hepatoblasts more efficiently on α1-containing laminin than on α5-containing laminin. Hepatoblasts were isolated from E14.5 liver and cultured on dishes coated with α1-containing laminin (laminin 111) or α5-containing laminin (laminin 511). At day 3 of culture, cells were stimulated with 500 pg/ml TGFβ for 24 h. Gene expression was examined by quantitative PCR. Cultures were repeated three times independently. A *t* test was performed by Microsoft Excel software. *, $p < 0.05$. *HPRT*, hypoxanthine phosphoribosyltransferase; *PV*, portal vein. *Error bars* in *panels C*, *D* and *E* represent standard deviation.

CK19$^-$HNF4α$^+$ hepatoblasts on the other (Fig. 6*A*, *panels 9–12*). We found that the number of asymmetric ducts was increased in the mutant liver (supplemental Fig. 6), suggesting that tubular morphogenesis was attenuated at the middle of the tubular morphogenesis. On the other hand, it is not clear whether the smaller lumen is also caused by the delay of the morphogenesis. In fetal liver, in addition to mature and asymmetric immature ducts, double layered ductal plates associated with or without lumens are observed in late gestation, suggesting that lumens are generated between two layers and gradually increase their size along an alternative morphogenic pathway. Given that laminin α5 contributes to expansion of the luminal space *in vitro*, the lack of laminin α5 in cholangiocytes might reduce the size of lumen, which is generated between ductal plates through this type of morphogenic pathway.

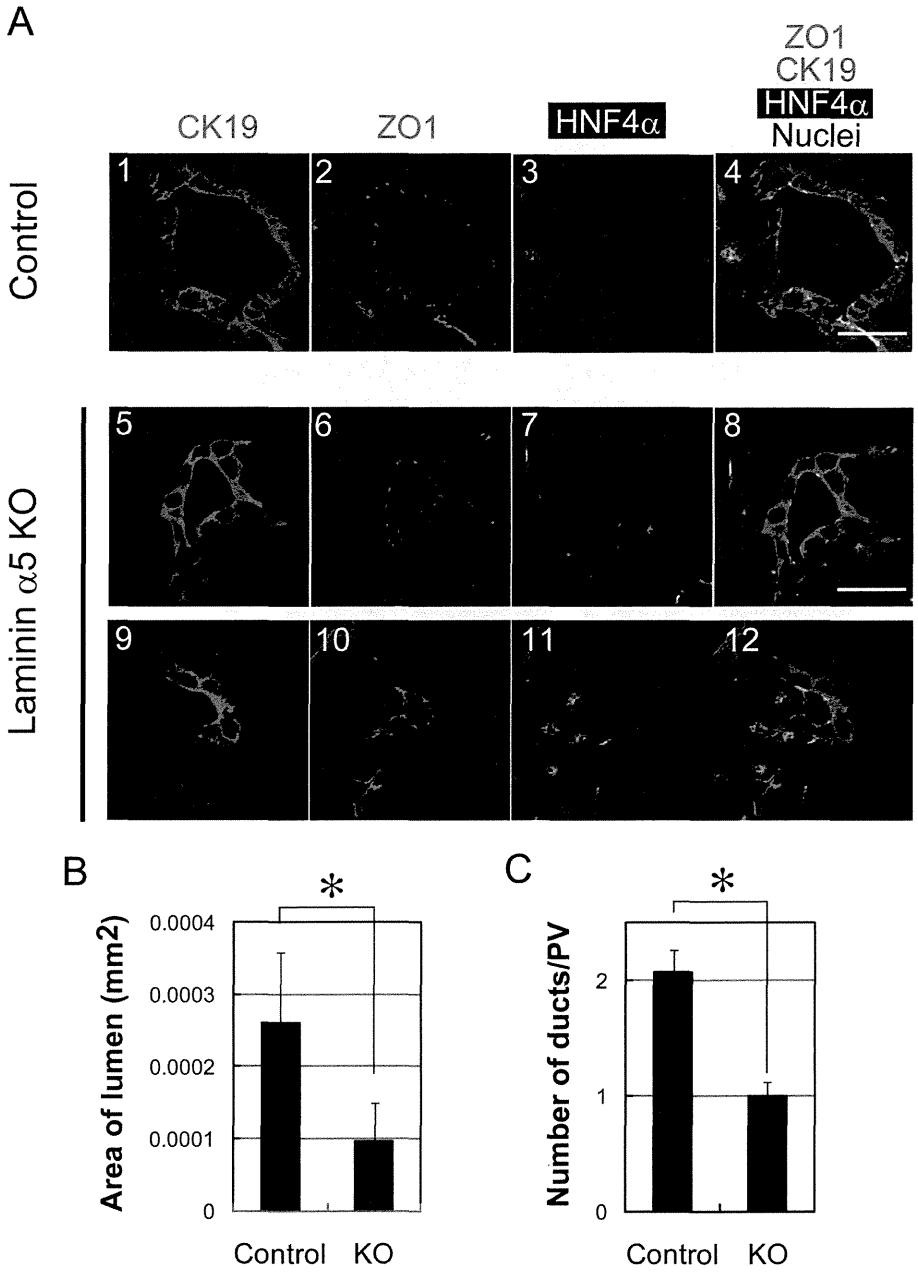

FIGURE 6. **Defects of bile duct formation in laminin α5 KO liver.** *A*, duct structures in the control and laminin α5 KO livers are characterized by the expression of CK19, ZO1, and HNF4α. All three duct structures are associated with a single lumen surrounded by cells with tight junctions recognized by ZO1 staining (*green*). Ducts in *panels 1–8* are totally surrounded by $CK19^{+}HNF4\alpha^{-}$ cholangiocytes. On the other hand, an immature duct in *panels 9–12* is surrounded by $CK19^{+}HNF4\alpha^{-}$ cholangiocytes and $CK19^{-}HNF4\alpha^{+}$ hepatoblasts. *B*, the lumen size of the bile duct is reduced in laminin α5 KO liver. The lumen surrounded with $CK19^{+}$ cholangiocytes was selected, and its area was measured by ImageJ. A *t* test was performed by Microsoft Excel software. *, $p < 0.05$. *C*, the number of duct structures is reduced in laminin α5 KO liver. $CK19^{+}$ duct structures around the portal vein were counted in more than 10 sections in each liver tissue. More than 50 portal areas were examined for each embryonic liver. A *t* test was performed by Microsoft Excel software. *, $p < 0.05$. *Scale bars* represent 20 μm. *Error bars* represent standard deviation.

It is known that α1-containing laminin is abundant in fetal tissues but not in adult tissues. By contrast, α5-containing laminin is a major component of basal lamina in mature epithelial tissues. Although laminins α1 and α5 are structurally similar, recent reports demonstrated that α5-containing laminin has some unique functions that cannot be substituted for by α1-containing laminin. Kikkawa and Miner (26) generated laminin α5 KO mice expressing a mutant laminin α5 chain in which the entire α5 laminin globular domain was replaced by α1 laminin globular domain and showed that the mutant laminin α5 chain failed to rescue the developmental defects observed in α5 KO mice. Gao *et al.* (27) demonstrated that α1-containing laminin failed to rescue the defects in hair follicle morphogenesis in laminin α5 KO mice. Our data revealed a novel function of α5-containing laminin in tubular morphogenesis of bile ducts, suggesting that α5-containing laminin

might be involved in epithelial morphogenesis of other epithelial tubular structures in the lung, kidney, reproductive organs, and pancreas.

Our data show that among β1 integrins α6β1 integrin works as a receptor for laminins during cyst morphogenesis of HPPL. In addition to α6, HPPL expresses α3 subunit. Although it remains to be proven that α3 integrin is definitely involved in cyst morphogenesis, because anti-α6 antibody did not completely inhibit cyst morphogenesis, α3 integrin may be another partner of β1 integrin. In contrast to the basal localization of β1 integrin (Fig. 1*A*), β4 integrin in the basal domain was not clear at the beginning of the culture (supplemental Fig. 1A). We also found the expression of β1 integrin in $Sox9^+$ cholangiocytes at E16.5 (supplemental Fig. 2A, arrowheads), whereas most of the $Sox9^+$ cells did not express β4 integrin (supplemental Fig. 2C). These results suggested that β4 integrin signals might be involved in the latter process of bile duct morphogenesis or the maintenance of the structure but not in the establishment of apicobasal polarity. However, β4 integrin signaling is not essential for the maintenance of the cyst structure because anti-β4 antibody only slightly disrupted the cyst structure (supplemental Fig. 1C). Thus, β1 integrin mainly mediates signals from laminins in HPPL during and after the cyst formation in three-dimensional culture.

β1 integrin has been shown to play important roles for epithelial cells to receive ECM signals (15–19). Blocking the function of β1 integrin resulted in dissolution of the cyst structure, but the polarity was not completely dissolved; the apical markers were not randomly localized but faced the ECM, and tight junctions were formed at cell-cell contacts near the ECM. A similar phenotype has been described in three-dimensional culture of Madin-Darby canine kidney cells (15, 28) and in the *Drosophila* ovary (29) and is considered to be "inverted polarity." However, in the culture of HPPL, anti-β1 integrin induced inverted polarity in the presence of exogenous laminin. By contrast, Madin-Darby canine kidney cells could form the normal apicobasal polarity by the addition of exogenous laminin even in the presence of anti-β1 antibody. The difference might be explained by the fact that Madin-Darby canine kidney cells may express an unknown laminin receptor that is not expressed in HPPL.

In summary, we have demonstrated that the formation of apicobasal polarity and lumen, progression of tubular morphogenesis, and maintenance of the proper bile duct structure require signaling by β1 integrin that is sequentially activated by α1-containing laminin provided via mesenchymal cells and then α5-containing laminin expressed by cholangiocytes themselves. It was reported that laminin and type IV collagen, two major components of the basal lamina, were reduced or partly lost around bile ducts in congenital hepatic fibrosis and Caroli disease and in the PCK rat liver, an animal model of Caroli disease (30). Thus, the interactions between laminin and cholangiocytes may also be important for preventing the pathogenesis of fibrosis. However, it has remained unknown how the degeneration of the basal lamina leads to fibrosis. In three-dimensional culture, the layer of basal laminin was disrupted in parallel with the loss of polarity (supplemental Fig. 7). By inhibiting the interaction between ECM and epithelial cells in three-dimensional culture of HPPL, it may be possible to obtain critical information on the link between the loss of integrity of the basal lamina and the pathogenesis of fibrosis in epithelial tissues.

Acknowledgments—We thank Dr. Takako Sasaki for providing antibodies against laminins α1 and α5. We also thank Dr. Jeff H. Miner for providing liver tissues of laminin α5 KO mice. We appreciate the valuable technical assistance of Shigeru Saito, Minako Kuwano, and Yumiko Tsukamoto. We thank the members of the laboratories of Prof. Miyajima and Prof. Mitaka for helpful discussions.

REFERENCES

1. Shiojiri, N. (1997) Development and differentiation of bile ducts in the mammalian liver. *Microsc. Res. Tech.* **39,** 328–335
2. Lemaigre, F. P. (2003) Development of the biliary tract. *Mech. Dev.* **120,** 81–87
3. Antoniou, A., Raynaud, P., Cordi, S., Zong, Y., Tronche, F., Stanger, B. Z., Jacquemin, P., Pierreux, C. E., Clotman, F., and Lemaigre, F. P. (2009) Intrahepatic bile ducts develop according to a new mode of tubulogenesis regulated by the transcription factor SOX9. *Gastroenterology* **136,** 2325–2333
4. Zong, Y., Panikkar, A., Xu, J., Antoniou, A., Raynaud, P., Lemaigre, F., and Stanger, B. Z. (2009) Notch signaling controls liver development by regulating biliary differentiation. *Development* **136,** 1727–1739
5. Sanzen, T., Harada, K., Yasoshima, M., Kawamura, Y., Ishibashi, M., and Nakanuma, Y. (2001) Polycystic kidney rat is a novel animal model of Caroli's disease associated with congenital hepatic fibrosis. *Am. J. Pathol.* **158,** 1605–1612
6. Martin-Belmonte, F., Gassama, A., Datta, A., Yu, W., Rescher, U., Gerke, V., and Mostov, K. (2007) PTEN-mediated apical segregation of phosphoinositides controls epithelial morphogenesis through Cdc42. *Cell* **128,** 383–397
7. Kesavan, G., Sand, F. W., Greiner, T. U., Johansson, J. K., Kobberup, S., Wu, X., Brakebusch, C., and Semb, H. (2009) Cdc42-mediated tubulogenesis controls cell specification. *Cell* **139,** 791–801
8. Colognato, H., and Yurchenco, P. D. (2000) Form and function: the laminin family of heterotrimers. *Dev. Dyn.* **218,** 213–234
9. Miner, J. H., and Yurchenco, P. D. (2004) Laminin functions in tissue morphogenesis. *Annu. Rev. Cell Dev. Biol.* **20,** 255–284
10. Durbeej, M. (2010) Laminins. *Cell Tissue Res.* **339,** 259–268
11. Kikkawa, Y., Mochizuki, Y., Miner, J. H., and Mitaka, T. (2005) Transient expression of laminin α1 chain in regenerating murine liver: restricted localization of laminin chains and nidogen-1. *Exp. Cell Res.* **305,** 99–109
12. Kikkawa, Y., Sudo, R., Kon, J., Mizuguchi, T., Nomizu, M., Hirata, K., and Mitaka, T. (2008) Laminin α5 mediates ectopic adhesion of hepatocellular carcinoma through integrins and/or Lutheran/basal cell adhesion molecule. *Exp. Cell Res.* **314,** 2579–2590
13. Shiojiri, N., and Sugiyama, Y. (2004) Immunolocalization of extracellular matrix components and integrins during mouse liver development. *Hepatology* **40,** 346–355
14. Tanimizu, N., Miyajima, A., and Mostov, K. E. (2007) Liver progenitor cells develop cholangiocyte-type epithelial polarity in three-dimensional culture. *Mol. Biol. Cell* **18,** 1472–1479
15. Yu, W., Datta, A., Leroy, P., O'Brien, L. E., Mak, G., Jou, T. S., Matlin, K. S., Mostov, K. E., and Zegers, M. M. (2005) β1-integrin orients epithelial polarity via Rac1 and laminin. *Mol. Biol. Cell* **16,** 433–445
16. Rebustini, I. T., Patel, V. N., Stewart, J. S., Layvey, A., Georges-Labouesse, E., Miner, J. H., and Hoffman, M. P. (2007) Laminin α5 is necessary for submandibular gland epithelial morphogenesis and influences FGFR expression through β1 integrin signaling. *Dev. Biol.* **308,** 15–29
17. Zhang, X., Mernaugh, G., Yang, D. H., Gewin, L., Srichai, M. B., Harris, R. C., Iturregui, J. M., Nelson, R. D., Kohan, D. E., Abrahamson, D., Fässler, R., Yurchenco, P., Pozzi, A., and Zent, R. (2009) β1 integrin is necessary for ureteric bud branching morphogenesis and maintenance of collecting

duct structural integrity. *Development* **136,** 3357–3366
18. Bombardelli, L., Carpenter, E. S., Wu, A. P., Alston, N., DelGiorno, K. E., and Crawford, H. C. (2010) Pancreas-specific ablation of β1 integrin induces tissue degeneration by disrupting acinar cell polarity. *Gastroenterology* **138,** 2531–2540, 2540.e1–4
19. Myllymaki, S. M., Teräväinen, T. P., and Manninen, A. (2011) Two distinct integrin-mediated mechanisms contribute to apical lumen formation in epithelial cells. *PLoS One* **6,** e19453
20. Kikkawa, Y., Sasaki, T., Nguyen, M. T., Nomizu, M., Mitaka, T., and Miner, J. H. (2007) The LG1–3 tandem of laminin α5 harbors the binding sites of Lutheran/basal cell adhesion molecule and α3β1/α6β1 integrins. *J. Biol. Chem.* **282,** 14853–14860
21. Tanimizu, N., Nishikawa, M., Saito, H., Tsujimura, T., and Miyajima, A. (2003) Isolation of hepatoblasts based on the expression of Dlk/Pref-1. *J. Cell Sci.* **116,** 1775–1786
22. Tanaka, M., Okabe, M., Suzuki, K., Kamiya, Y., Tsukahara, Y., Saito, S., and Miyajima, A. (2009) Mouse hepatoblasts at distinct developmental stages are characterized by expression of EpCAM and DLK1: drastic change of EpCAM expression during liver development. *Mech. Dev.* **126,** 665–676
23. Suzuki, K., Tanaka, M., Watanabe, N., Saito, S., Nonaka, H., and Miyajima, A. (2008) p75 neurotrophin receptor is a marker for precursors of stellate cells and portal fibroblasts in mouse fetal liver. *Gastroenterology* **135,** 270–281.e3
24. Okabe, M., Tsukahara, Y., Tanaka, M., Suzuki, K., Saito, S., Kamiya, Y., Tsujimura, T., Nakamura, K., and Miyajima, A. (2009) Potential hepatic stem cells reside in EpCAM$^+$ cells of normal and injured mouse liver. *Development* **136,** 1951–1960
25. Sorokin, L. M., Pausch, F., Durbeej, M., and Ekblom, P. (1997) Differential expression of five laminin α (1–5) chains in developing and adult mouse kidney. *Dev. Dyn.* **210,** 446–462
26. Kikkawa, Y., and Miner, J. H. (2006) Molecular dissection of laminin α5 *in vivo* reveals separable domain-specific roles in embryonic development and kidney function. *Dev. Biol.* **296,** 265–277
27. Gao, J., DeRouen, M. C., Chen, C. H., Nguyen, M., Nguyen, N. T., Ido, H., Harada, K., Sekiguchi, K., Morgan, B. A., Miner, J. H., Oro, A. E., and Marinkovich, M. P. (2008) Laminin-511 is an epithelial message promoting dermal papilla development and function during early hair morphogenesis. *Genes Dev.* **22,** 2111–2124
28. Yu, W., Shewan, A. M., Brakeman, P., Eastburn, D. J., Datta, A., Bryant, D. M., Fan, Q. W., Weiss, W. A., Zegers, M. M., and Mostov, K. E. (2008) Involvement of RhoA, ROCK I and myosin II in inverted orientation of epithelial polarity. *EMBO Rep.* **9,** 923–929
29. Fernández-Miñán, A., Cobreros, L., González-Reyes, A., and Martín-Bermudo, M. D. (2008) Integrins contribute to the establishment and maintenance of cell polarity in the follicular epithelium of the *Drosophila* ovary. *Int. J. Dev. Biol.* **52,** 925–932
30. Yasoshima, M., Sato, Y., Furubo, S., Kizawa, K., Sanzen, T., Ozaki, S., Harada, K., and Nakanuma, Y. (2009) Matrix proteins of basement membrane of intrahepatic bile ducts are degraded in congenital hepatic fibrosis and Caroli's disease. *J. Pathol.* **217,** 442–451

Grainyhead-like 2 regulates epithelial morphogenesis by establishing functional tight junctions through the organization of a molecular network among claudin3, claudin4, and Rab25

Kazunori Senga[a,*], Keith E. Mostov[b], Toshihiro Mitaka[c], Atsushi Miyajima[a], and Naoki Tanimizu[a,b,c,*]
[a]Institute of Molecular and Cellular Biosciences, University of Tokyo, 1-1-1 Yayoi, Bunkyo-ku, Tokyo 113-0032 Japan; [b]Department of Anatomy and Department of Biochemistry and Biophysics, University of California, San Francisco, San Francisco, CA 94143-2140; [c]Department of Tissue Development and Regeneration, Research Institute for Frontier Medicine, Sapporo Medical University School of Medicine, S-1, W-17, Chuo-ku, Sapporo 060-8556, Japan

ABSTRACT During development, epithelial progenitors establish intercellular junctions, including tight junctions (TJs), and form three-dimensional (3D) tissue structures, which are often associated with luminal structures. Here we identify grainyhead-like 2 (Grhl2) as a transcription factor that regulates the size of luminal space surrounded by polarized epithelial cells. We show that HPPL, a liver progenitor cell line, transfected with Grhl2 cDNA forms remarkably larger cysts than the control cells in 3D cultures. We find that Grhl2 up-regulates claudin (Cldn) 3 and Cldn4, and their functions are necessary for the formation of large cysts. Overexpression of Cldn3 alone induces the cyst expansion. In contrast, expression of Cldn4 alone does not induce expansion, as it is not localized at TJs. Of interest, Rab25, another Grhl2 target, not only increases the Cldn4 protein, but also enhances its localization at TJs. Taken together, the results indicate that Grhl2 regulates epithelial morphogenesis through transcriptional up-regulation of Cldn3 and Cldn4, as well as of Rab25, which increases the Cldn4 protein and its localization at TJs. The results reveal a molecular network regulating epithelial lumen formation organized by Grhl2.

Monitoring Editor
Asma Nusrat
Emory University

Received: Feb 8, 2012
Revised: Jun 4, 2012
Accepted: Jun 7, 2012

INTRODUCTION

Epithelial cells are polarized and form tissue structures required for epithelial organs to perform their physiological functions. Cultured cells have been used to study molecular mechanisms underlying epithelial polarization and tissue morphogenesis (Bryant and Mostov, 2008; Martin-Belmonte and Mostov, 2008; Gray *et al.*, 2010). However, since cell lines used in those studies, such as Mardin–Darby canine kidney (cells or Caco-2 and MCF7 tumor cells, were mostly generated from adult tissues, the processes and mechanisms by which epithelial progenitor cells establish apicobasal polarity and form tissue structures during organogenesis remained largely unknown.

In the liver, two types of epithelial cells—hepatocytes and cholangiocytes—form hepatic cords and bile ducts, respectively. Bile ducts are tubular structures connecting the liver to the small intestine to drain bile secreted from hepatocytes. Bile ducts are lined by cholangiocytes, which modulate the composition of the bile by secreting water and ions (Fitz, 2002). For proper function of the liver, the bile composition needs to be strictly controlled, and any leakage of cytotoxic bile into the parenchyma must be prevented while the bile flows through the liver tissue. Given those physiological functions, establishment of tight junctions (TJs) that control paracellular efflux of small substances is a critical step during the development of bile ducts. Around embryonic day 15 (E15), hepatoblasts—fetal liver stem cells—differentiate into cholangiocytes near the portal vein and form the ductal plate, a single layer of cholangiocytes, which is subsequently reorganized to form tubular structures (Lemaigre, 2003). At an early stage of the reorganization of the ductal plate, cholangiocytes form TJs recognized by ZO1 expression (Antoniou *et al.*, 2009; Zong *et al.*, 2009). However, it remains

This article was published online ahead of print in MBoC in Press (http://www.molbiolcell.org/cgi/doi/10.1091/mbc.E12-02-0097) on June 13, 2012.

*These authors contributed equally to this work.

Address correspondence to: Naoki Tanimizu (tanimizu@sapmed.ac.jp).

Abbreviations used: 3D, three-dimensional; Cldn, claudin; CPE, *Clostridium perfringens* enterotoxin; Grhl2, grainyhead-like 2; TJ, tight junction.

unknown whether those TJs are functional and how immature cholangiocytes establish mature TJs.

Comparison of gene expression profiles between epithelial cells and their progenitors may be an effective way to identify genes regulating epithelial morphogenesis. In this study, we compared neonatal cholangiocytes, which are undergoing tubular morphogenesis, with hepatoblasts by microarray and identified grainyhead-like 2 (Grhl2) as a transcription factor specifically expressed in cholangiocytes. Furthermore, by studying functions of Grhl2 and its target genes in three-dimensional (3D) culture system of liver progenitor cells, we revealed a novel molecular pathway conferring TJ integrity on epithelial progenitors and regulating epithelial morphogenesis.

RESULTS

Comparison of gene expression profiles between hepatoblasts and cholangiocytes isolated from developing liver

Epithelial cells form 3D tissue structures in many organs. In 3D culture, they form cysts, spherical structures with the central lumen surrounded by the polarized epithelial monolayer (Zegers *et al.*, 2003). HPPL, a liver progenitor cell line, can form such cysts in 3D culture (Tanimizu *et al.*, 2007). However, we realized that, compared with mature cholangiocytes isolated from adult mouse liver, HPPL formed cysts with much smaller lumens (Figure 1A), suggesting that HPPL may lack a critical factor inducing characteristics of mature epithelial cells, such as the formation of cysts with a large central lumen. Because tubular structures with apical lumen become evident around the portal vein in the late gestation and the neonatal stages, we considered the possibility that genes up-regulated in cholangiocytes in these developmental stages might play a role in the formation and/or maturation of luminal structures. To identify key molecules in the formation and/or maturation of luminal structures of tubular ducts, we isolated hepatoblasts (fetal liver stem cells) and neonatal cholangiocytes based on the expression of Dlk and EpCAM, respectively (Supplemental Figure S1) and performed a microarray analysis to identify genes preferentially expressed in cholangiocytes undergoing tubular morphogenesis (Supplemental Tables S1 and S2).

Grainyhead-like 2 enhances epithelial characteristics of liver progenitor cells

Among those genes up-regulated in cholangiocytes, we focused on transcription factors, ankyrin repeat domain 1 (Ankrd1), ets homologous factor (Ehf), grainyhead-like 2 (Grhl2), hairy/enhancer-of-split related with YRPW motif 1 (Hey1), and scleraxis (Scx) as candidate genes regulating epithelial morphogenesis of cholangiocytes. To find a gene implicated in increasing the lumen size, we overexpressed each transcription factor in HPPL and performed 3D culture. We found that only Grhl2 remarkably increased the lumen size of HPPL cysts (Figure 1, B and C).

Grhl2 is a mammalian homologue of *Drosophila* grainyhead, which is implicated in epithelial morphogenesis (Werth *et al.*, 2010; Pyrgaki *et al.*, 2011). However, expression of Grhl2 in the liver and its functions during the development of epithelial organs, including the liver, has not been reported. First, we performed quantitative PCR and confirmed the expression of Grhl2 in EpCAM$^+$ cholangiocytes at both P0 and adult stages (Supplemental Figure S2A). We also examined the expression of Grhl1 and Grhl3, the other members of the mammalian grainyhead family, and confirmed that only Grhl2 was expressed in cholangiocytes (Supplemental Figure S2B). Next we immunohistochemically examined the expression of Grhl2 in E17.5, P1, and P8 livers. Grhl2 was detected in the nuclei of EpCAM$^+$ cholangiocytes in P1 and P8 livers (Figure 1D, 4–9), whereas it was not expressed in E17.5 liver, where most cholangiocytes form ductal plates (Figure 1D, 1–3). These results suggested that Grhl2 is not involved in the differentiation of cholangiocytes from bipotential hepatoblasts, but it might regulate a later stage, that is, structural and/or functional maturation of bile ducts.

Grhl2 enlarges the lumen without promoting cell proliferation

Because large cysts derived from HPPL expressing Grhl2 (HPPL-Grhl2) apparently consisted of more cells than those from the control HPPL (Figure 1C), increased proliferation might result in large lumens. Actually, at day 7, the lumens of HPPL-Grhl2 cysts consisted of more cells as compared with the control cysts (Figure 2A). On the other hand, a similar number of cells formed the lumens of the control and HPPL-Grhl2 cysts at day 4 (Figure 2B). We monitored the process of lumen expansion from day 2.5 of 3D culture under a microscope and found that HPPL-Grhl2 rapidly expanded the lumen without changing the number of cells (Figure 2C). Thus it is unlikely that Grhl2-induced expansion of lumen was promoted by cell proliferation.

Grhl2 enhances epithelial barrier by up-regulating the expression of Cldn3 and Cldn4

Epithelial cells establish intercellular junctions, including TJs, during development. Although the correlation between the formation of TJs and epithelial morphogenesis has not been adequately clarified, we considered the possibility that maturation of TJs might be coupled with the expansion of a central lumen of cysts. A major physiological function of TJs is forming the paracellular epithelial barrier. We examined the permeability of dextran through the monolayer, which has been used to verify the formation of the epithelial barrier. The results showed that adult cholangiocytes and HPPL-Grhl2 that formed large cysts established a monolayer with strong barrier function as compared with the control HPPL (Figure 3, A and B). Among components of TJs, claudins (Cldns) regulate paracellular permeability of small substances, including ions, by forming paracellular channels (Tsukita and Furuse, 2002). The microarray data indicated that Cldn2, 3, 4, 6, 7, and 8 might be up-regulated when hepatoblasts differentiate to cholangiocytes (Supplemental Table S3). Therefore we addressed whether those molecules mediate the function of Grhl2. First, we compared the expression of these Cldns in HPPL-Grhl2 with that in the control HPPL and found that mRNA levels of Cldn3, 4, and 8 were slightly increased by Grhl2 (Figure 3C). Of interest, Cldn3 and 4 proteins were clearly increased by Grhl2 (Figure 3D). They were detected in the Triton X-100–soluble fraction and also the insoluble fraction, in which TJ proteins are enriched (Figure 3E). Furthermore, immunocytochemistry revealed that Cldn3 and 4 proteins were colocalized with ZO1 at cell–cell contacts, indicating that both are at TJs in HPPL-Grhl2 (Figure 3, F and G). These results suggested that Grhl2 promoted the barrier function of bile ducts by up-regulating Cldn3 and 4 proteins.

Grhl2 expands the lumen of HPPL cysts via Cldn3 and Cldn4

Next, to examine roles of claudins in lumen formation, we took advantage of 3D culture of HPPL. We examined localization of Cldn3 and 4 in cysts derived from HPPL-Grhl2 and found that they were colocalized with ZO1, indicating their localization at TJs (Figure 4A). Then, we added the C-terminal peptide derived from *Clostridium perfringens* enterotoxin (C-CPE), which has been shown to bind Cldn3, 4, and 6 and inhibit their function (Moriwaki *et al.*, 2007). glutathione *S*-transferase (GST)–C-CPE peptide excluded Cldn3 and 4 from TJs (unpublished data). In the presence of the GST-fusion protein of C-CPE peptide, HPPL-Grhl2 formed smaller lumens

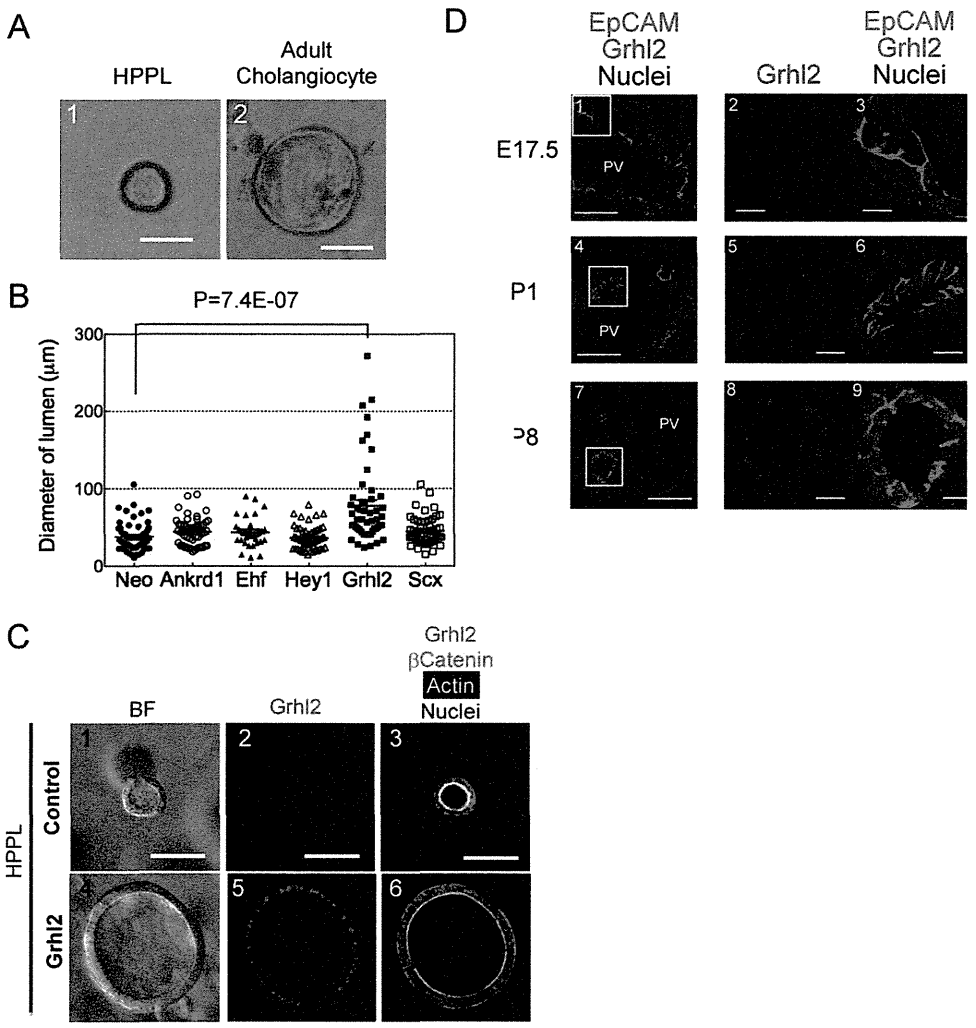

FIGURE 1: Grhl2 enlarges the central lumen of cysts. (A) Mature cholangiocytes form larger cysts than HPPL. Mature cholangiocytes were isolated from mouse adult liver based on the expression of EpCAM. EpCAM$^+$ cholangiocytes and HPPL were cultured in gel containing Matrigel for 7 d. Bar, 50 μm. (B) Effects of transcription factors on the size of a central lumen. HPPL were introduced with retrovirus containing cDNA of Ankrd1, EHF, Hey1, Grhl2, or Scx and used for 3D culture. After 7 d of incubation, pictures were taken for at least 20 areas for measuring the size of cysts. A dot plot with bars of mean ± SEM for a representative culture indicates that the diameter of lumen derived from HPPL expressing Grhl2 (HPPL-Grhl2) is larger than the control with statistical significance. (C) Cyst structures in 3D culture of control HPPL and HPPL-Grhl2. Both HPPL and HPPL-Grhl2 cysts show apical actin bundles (white) and basal β-catenin (green), whereas cysts derived from HPPL-Grhl2 have remarkably larger lumen (4–6) as compared with the control (1–3). The control HPPL and HPPL-Grhl2 were cultured in gel containing Matrigel for 7 d. Cysts were incubated with anti-Grhl2 and anti–β-catenin antibodies, followed by incubation with secondary antibodies and Alexa Fluor 633–conjugated phalloidin. Nuclei were counterstained with Hoechst 34580. BF, bright field. Bars, 50 μm. (D) Immunofluorescence analysis of Grhl2 expression in developing liver. In E17.5 liver (1–3), Grhl2 (red) is not detectable in EpCAM$^+$ cholangiocytes (green), whereas it is expressed in cholangiocytes forming tubular structures in P1 (4–6) and P8 (7–9). Boxes in 1, 4, and 7 are enlarged in 2/3, 5/6, and 8/9, respectively. Bars, 50 μm (1, 4, and 7), 10 μm (2, 3, 5, 6, 8, and 9).

compared with the culture with C-CPE313 peptide, an inactive mutant (Figure 4, B and C). Thus functions of Cldns were indispensable for the Grhl2-induced enlargement of cysts.

We also overexpressed Cldn3 or Cldn4 in HPPL (Supplemental Figures S3 and S4). As shown in Figure 4, D and E, Cldn3 alone, but not Cldn4, increased the size of lumen. Moreover, cysts derived from HPPL-Cldn3+4 formed lumens similar in size to those derived from HPPL-Cldn3 (Supplemental Figure S5). We found that Cldn4 was not localized at TJs in HPPL-Cldn4 (see later discussion of Figure 6), which provides a possible explanation for why expression of Cldn4 alone did not increase the size of lumen. On the other hand, Cldn4 was localized at TJs in HPPL-Grhl2 (Figure 4A, 13–16), suggesting that an additional factor induced by Grhl2 may be necessary for Cldn4 to be localized at TJs and thereby be functional (see later discussion).

Grhl2 enlarges the central lumen of cysts by up-regulating Rab25

Because the expression of Cldn3 and 4 was not sufficient to mimic the effect of Grhl2 on lumen size, other targets of Grhl2 were likely to be involved. The consensus DNA sequence for Grhl2 binding was

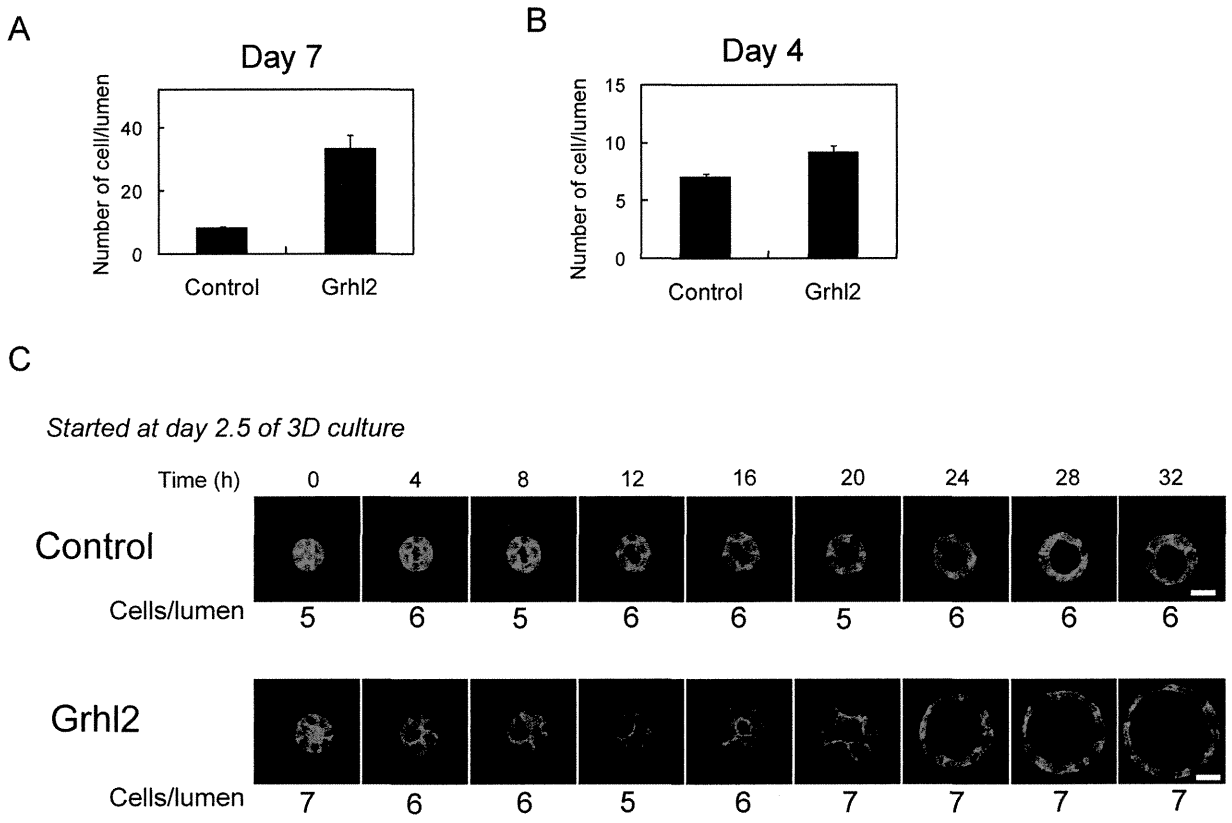

FIGURE 2: HPPL-Grhl2 starts expanding the lumen without proliferation. (A) Cysts derived from HPPL-Grhl2 contain more cells than the control at day 7 of 3D culture. Cysts were fixed in 4% PFA, and nuclei were stained with Hoechst 34580. Pictures were taken on a microscope, and the number of cells surrounding the lumen was counted. (B) Cysts derived from HPPL-Grhl2 contain similar number of cells at day 4 of 3D culture. (C) HPPL-Grhl2 expands the lumen without changing the number of cells forming the lumen. Images of cysts derived from the control HPPL and HPPL-Grhl2 at different time points were taken under a confocal microscope. The numbers of cells around the lumen are indicated under the image at each time point. Bars, 50 μm.

reported as AACCGGTT (Werth *et al.*, 2010). Using a database of mouse and human genomes, we searched for genes that have this sequence in the proximal promoter (within 1000 base pairs from the transcription initiation site) in both mice and humans. Furthermore, we analyzed whether candidate genes were up-regulated in neonatal cholangiocytes as compared with hepatoblasts in the microarray data to find Grhl2 targets important for the enlargement of lumen (Supplemental Table S4). As a result, we identified several genes, including the small GTPase Rab25, as possible targets of Grhl2 (Figure 5A). We further confirmed that Rab25 was specifically up-regulated in the cholangiocyte lineage during in vivo bile duct development, and it was significantly increased by overexpression of Grhl2 (Supplemental Figure S6). There is one putative binding site for Grhl2 (Grhl2-binding element; GBE in Figure 5B) and one similar sequence (GBE? in Figure 5B) within 150 base pairs upstream of the transcription site. Promoter reporter assays using deletion mutants of the promoter region revealed that the putative binding site was necessary for Grhl2 to promote transcription (Figure 5B). These data strongly suggested that Rab25 is a target of Grhl2.

Next we established HPPL-Rab25, and their 3D culture showed that Rab25 increased lumen size (Figure 5, C and D). In contrast, a dominant-negative form of Rab25 partially inhibited the expansion of a central lumen induced by Grhl2 (Figure 5, E and F). These results suggested that Grhl2 regulated epithelial morphogenesis of HPPL through Rab25.

Rab25 increases Cldn4 protein and regulates its localization at TJs

We considered the possibility that Rab25 might regulate the expression and intracellular localization of Cldn4. Indeed, we found that Rab25 overexpression resulted in an increase of Cldn4 protein (Figure 6A), although it did not increase Cldn3 protein. Because Rab25 limited paracellular permeability of 4-kDa fluorescein isothiocyanate (FITC)–dextran (Figure 6B), Cldn4 in HPPL-Rab25 might be functional at TJs. We further performed immunofluorescence analysis and found colocalization of Cldn4 and ZO1 in cysts formed from HPPL-Rab25 (Figure 6C). Quantitative analysis confirmed that Rab25 induced colocalization of Cldn4 and ZO1 (Figure 6D and Supplemental Figure S7). By contrast, Cldn4 was mostly localized at the basolateral domain in HPPL-Cldn4. Consistently, dominant-negative Rab25 abolished colocalization of Cldn4 and ZO1 (Figure 6, E and F). These data indicated that Rab25 regulates the barrier function and morphogenesis of liver progenitor cells by up-regulating Cldn4 at TJs.

Molecular link among Cldn3, Cldn4, and Rab25

Grhl2 enhances the epithelial characteristics of HPPL through Cldn3, Cldn4, and Rab25. However, it was not clear how much the Grhl2 functions depend on these three molecules. Although Grhl2 up-regulates Cldn4 at the transcriptional level, the data in Figure 5 suggested that Cldn4 functions in HPPL depend on Rab25. Therefore we introduced both Cldn3 and Rab25 to HPPL (HPPL-Cldn3+Rab25)

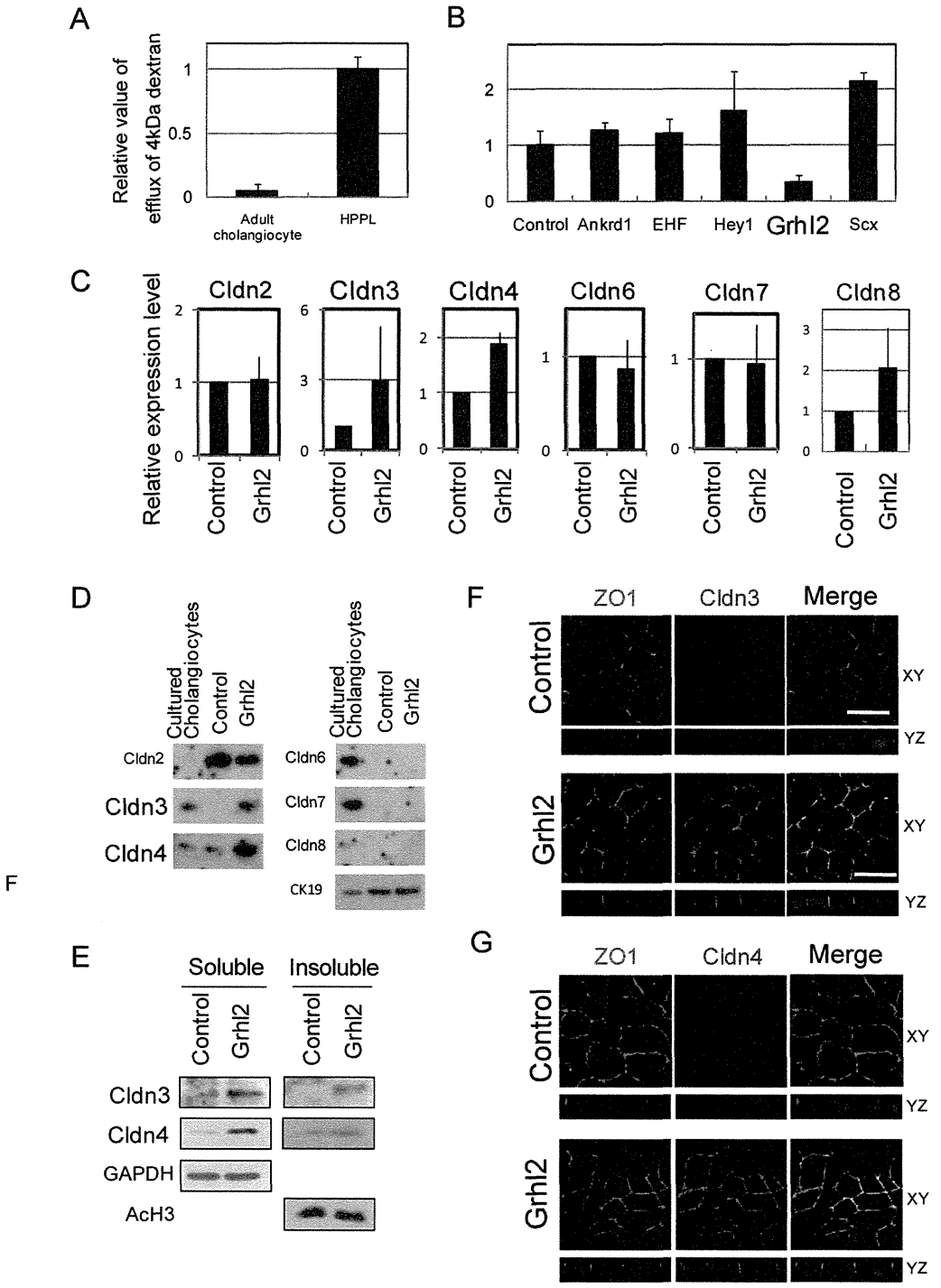

FIGURE 3: Grhl2 increases epithelial barrier function of HPPL by up-regulating Cldn3 and 4. (A) Adult mature cholangiocytes show stronger barrier functions than HPPL. Adult cholangiocytes were isolated as EpCAM$^+$ cells and plated onto a culture insert coated with type I collagen gel. HPPL were plated on a culture insert coated with laminin. FITC-dextran, 4 kDa, 1 mg/ml was added inside the culture insert, and 2 h later the medium in the bottom was used for measuring the fluorescence of FITC. (B) Grhl2 decreases the efflux of 4-kDa FITC-dextran through the monolayer of HPPL. (C) PCR analysis for expression of Cldn2, 3, 4, 6, 7, and 8. Cldn3, 4, and 8 are transcriptionally up-regulated by overexpression of Grhl2. (D) Western blot analysis for expression of Cldn2, 3, 4, 6, 7, and 8. Grhl2 increases Cldn3 and 4 proteins as compared with the control. (E) Detection of Cldn3 and 4 in Triton X-100–soluble and –insoluble fractions. Grhl2 increases Cldn3 and 4 proteins both in Triton X-100–insoluble fraction, which represents Cldns incorporated into TJs, and in soluble fraction. (F, G) Localization of Cldn3 and 4 in 2D culture. Cldn3 and 4 (red) are colocalized with ZO1 (green), suggesting that they are incorporated into TJs in HPPL-Grhl2. The monolayer of HPPL was stained with anti-ZO1 and either anti-Cldn3 or 4 antibody.

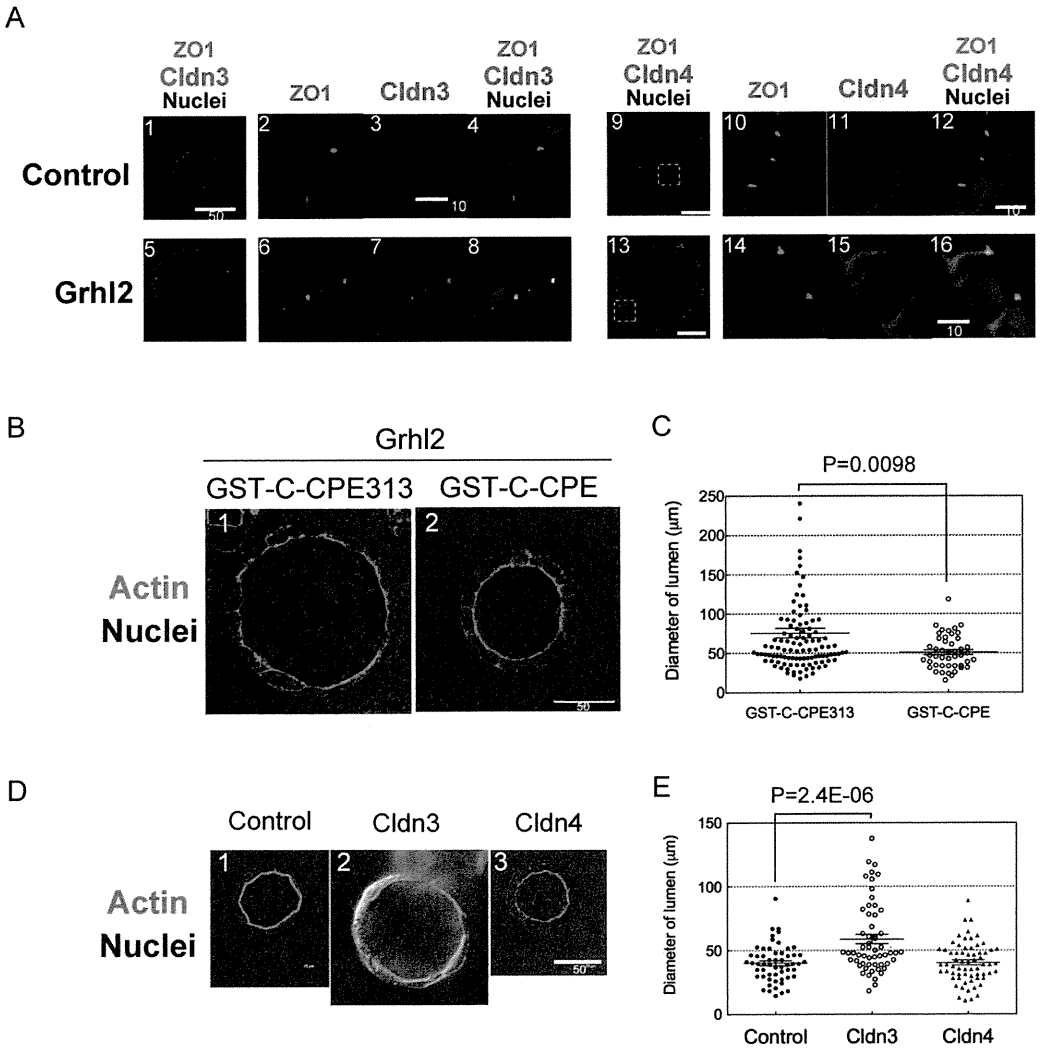

FIGURE 4: Cldn3 and 4 mediate the function of Grhl2 to enlarge a central lumen. (A) Cldn3 and 4 in HPPL-Grhl2 are localized at TJs. Cldn3 (red) expressed in HPPL-Grhl2 is colocalized with ZO1 (green; 5–8). Cldn4 (red) expressed in HPPL-Grhl2 is colocalized with ZO1 (green) in addition to relatively strong expression at the basolateral membrane (13–16). Cysts derived from HPPL and HPPL-Grhl2 were stained with anti-ZO1 and anti-Cldn3 or 4 antibodies. Nuclei were counterstained with Hoechst 34580 (blue). (B, C) Inhibition of Cldns by the C-terminal peptide derived from C-CPE decreases the size of a central lumen. Pictures for representative cysts are shown in B. The central lumen of cysts in the presence of CPE peptide is normally surrounded by F-actin bundle (green) but is remarkably smaller compared with the control. (C) Dot plot with bars of mean ± SEM for a representative culture, indicating that the lumen becomes smaller in the presence of CPE peptide with statistical significance. HPPL and HPPL-Grhl2 were cultured in the presence of 100 μg/ml GST-C-CPE or GST-C-CPE313 (a deletion mutant of C-CPE lacking the capability to bind to Cldns). The diameter of lumen was measured for >50 cysts per culture. Experiment was repeated four times independently. (D, E) Overexpression of Cldn3, but not Cldn4, induces the enlargement of a central lumen. (D) Representative pictures of cysts derived from HPPL, HPPL-Cldn3, and HPPL-Cldn4. Cldn3, but not Clnd4, enlarged the central lumen of a cyst. (E) Dot plot with bars of mean ± SEM for a representative culture, indicating that Cldn3 increases the size of lumen with statistical significance. HPPL, HPPL-Cldn3, and HPPL-Cldn4 were cultured under 3D conditions for 7 d. The diameter of lumen was measured for >50 cysts per culture. Experiment was repeated four times independently.

and examined the effect on epithelial properties of HPPL by comparing with HPPL-Cldn3 and HPPL-Rab25. HPPL-Cldn3+Rab25 significantly increased barrier function, as shown by the decrease in permeability of 4-kDa FITC-dextran (Figure 7A). In addition, in 3D culture, HPPL-Cldn3+Rab25 further increased the size of the central lumen (Figure 7C). The barrier function of HPPL-Cldn3+Rab25 was almost identical to that of HPPL-Grhl2 (Figure 7B). Thus Cldn3, Cldn4, and Rab25 are assumed to mediate the function of Grhl2 to regulate barrier functions of HPPL. However, as cysts derived from HPPL-Cldn3+Rab25 were still slightly smaller than those from HPPL-Grhl2 (Figure 7D), it remains possible that an additional Grhl2 target might be involved in enlargement of the central lumen of cysts.

DISCUSSION

Many epithelial tissues contain a luminal space. Paucity of lumen formation results in abnormal organ development, whereas

uncontrolled expansion of luminal space is observed in polycystic diseases. Thus it is important to regulate the size of lumen. However, in contrast to the initiation of lumen formation, molecular mechanisms regulating the size of lumen remain largely unknown. In this study, we compared neonatal cholangiocytes with hepatoblasts by microarray and identified genes specifically up-regulated in cholangiocytes. Among those genes, we found that a transcription factor, Grhl2, expands the apical luminal space of cysts derived from liver progenitor cells through up-regulation of Cldn3, Cldn4, and Rab25. Because Cldn3 and Cldn4, whose localization at TJs is regulated by Rab25, induce the maturation of TJs, our results linked the establishment of epithelial junctional complexes with the promotion of morphogenesis, in particular, lumen formation.

Grhl2 is a member of the grainyhead transcription factor family, mammalian homologues of *Drosophila* grainyhead. The mammalian grainyhead family consists of three members—Grhl1, 2, and 3. It has been demonstrated that Grhl1 regulates hair anchorage and epidermal differentiation (Wilanowski *et al.*, 2008), whereas Grhl3 regulates skin permeability by modulating the barrier function of epidermis, urothelial differentiation, and dorsal closure of the neural tube (Yu *et al.*, 2008, 2009). Recently Grhl2 was shown to be a key transcription factor completing neural tube closure (Pyrgaki *et al.*, 2011; Werth *et al.*, 2010) and modulating the nature of cell–cell contacts by promoting the formation of the apical junctional complex (Werth *et al.*, 2010). On the other hand, since mice lacking Grhl2 die around E13.5 before the development of most epithelial organs, including the liver, the roles of Grhl2 in epithelial morphogenesis remain unknown. Our data indicating that Grhl2 enhances epithelial barrier function and morphogenesis of liver progenitor cells in vitro show the possibility that Grhl2 regulates structural and functional differentiation of epithelial tissues.

TJs contain Cldns, as well as occludin and junctional adhesion molecules. Among those TJ proteins, Cldns regulate the paracellular transport of small substances (Tsukita and Furuse, 2002). Our results indicate that Grhl2 regulates barrier function of bile ducts by up-regulating Cldn3 and 4. Ectopic expression of Cldn3 resulted in the localization of Cldn3 at TJs and the modest expansion of the central lumen. On the other hand, the introduction of Cldn4 alone did not affect the size of lumens, probably because most of Cldn4 was localized at the basolateral domain (Figure 6, C and D). Although it was previously reported that ectopic expression of Cldn4 resulted in its localization at TJs and increased epithelial barrier, epithelial progenitors such as HPPL might lack a transport system required for the proper localization of Cldn4. Our results show that the Grhl2-Rab25 axis plays a key role in barrier function by localizing Cldn4 at TJs.

Rab25 is a member of the Rab11 subfamily consisting of Rab11a, 11b, and 25. Rab11a and Rab25 are implicated in recycling of apical proteins (Casanova *et al.*, 1999). Rab25 is known to be relatively abundant in gastrointestinal tissues (Goldenring *et al.*, 1993). Recently it was reported that Rab11a and 25 are involved in the formation of apical lumens (Bryant *et al.*, 2010). Because HPPL can form small cysts without Rab25 in 3D culture, it may be dispensable for HPPL to form the apical lumen in our system. On the other hand, Rab25 contributes to the formation of mature epithelial structures by localizing Cldn4 at TJs. Given that Rab25-knockout mice did not show any defects in liver (Nam *et al.*, 2010), Rab11a and Rab25 may have a redundant function in the bile duct development. However, it might be worth examining whether bile ducts without Rab25 are more susceptible to any type of liver injury.

It remains unclear how the Grhl2-Rab25 axis up-regulates Cldn4 and promotes its localization at TJs. Given that Rab25 has been implicated in recycling of apical proteins, it may promote the transport of internalized Cldn4 protein back to TJs, leading to prevention of the traffic of Cldn4 to lysosomes for degradation. Furthermore, a recent article demonstrated that Rab25 but not Rab11a regulates the transcytosis of FcRn from the basolateral to the apical and vice versa (Tzaban *et al.*, 2009). Given that most of Cldn4 is localized at the basolateral domain, Rab25 might be involved in trafficking Cldn4 from the basolateral domain to TJs by transcytosis, possibly through indirect interactions between Rab25 and Cldn4 (Supplemental Figure S8).

We summarize a molecular network governed by Grhl2 in Figure 8. Grhl2 enhances epithelial barrier by up-regulating Cldn3 and Cldn4, which leads to lumen expansion. In addition, Grhl2 enhances lumen expansion by up-regulating Rab25, which up-regulates Cldn4 protein and also regulates its localization at TJs. Strong barrier function is probably a physiological requirement for bile duct tubules to prevent any leakage of cytotoxic bile into the liver parenchyma. In fact, it was recently shown in zebrafish that Cldn15 and Cldn15-like b were necessary for normal formation of intestine (Bagnat *et al.*, 2007) and bile ducts (Cheung *et al.*, 2011), respectively. Our results reveal a novel mechanism regulating the process by which epithelial cells acquire mature epithelial structures necessary for their physiological functions.

MATERIALS AND METHODS

Extracellular matrix, growth factors, and chemicals

Type I collagen was purchased from Koken (Tokyo, Japan). Growth factor–reduced Matrigel and purified laminin-1 were from BD Biosciences (Bedford, MA).

Cell preparation and RNA isolation

Liver cells were isolated from E14.5, E17.5, and P0 livers according to a previous report, with slight modification. Livers were minced and then digested in Librase 3 blenzyme (Roche Applied Science, Indianapolis, IN) that was 50 times diluted in phosphate-buffered saline (PBS) ++. Cells were incubated with anti-mouse EpCAM (BD Biosciences) conjugated with Alexa Flour 488 or FITC-conjugated anti-mouse EpCAM (Okabe *et al.*, 2009). $EpCAM^+$ cells were isolated with a FACSAria. Dlk^+ cells were isolated from E14.5 liver as previously reported (Tanimizu *et al.*, 2003).

Total RNA was isolated from purified Dlk^+ and $EpCAM^+$ cells by using a Purelink RNA mini kit (Ambion, Austin, TX). RNA concentration was measured on a NanoDrop (Thermo Fisher Scientific, Waltham, MA). After checking concentration, we checked the quality of RNA samples on a bioanalyzer (Agilent Technologies, Santa Clara, CA).

Microarray analysis

For comparing hepatoblasts and cholangiocytes, synthesis and labeling of cRNA were performed at the University of California, San Francisco, Sandler Center. Agilent whole genome mouse array (014868) was used for gene expression analysis.

Plasmids

cDNA of Grhl2 was amplified from Kazusa cDNA clone (kindly provided by Osamu Obara, Kazusa DNA Research Institute, Chiba, Japan). cDNAs of Ankrd1, Ehf1, Hey1, Scx, Cldn3, Cldn4, and Rab25 were amplified from first-strand cDNA synthesized from neonatal cholangiocytes or kidney. A dominant-negative form of Rab25 (dn-Rab25) was generated by adding a point mutation in its GTP-binding domain to change Thr26 to Gln (Casanova *et al.*, 1999). After performance of DNA sequencing, they were transferred to a retrovirus vector, pMXsNeo. Infected HPPL were treated with 0.1 mg/ml G418 to select cells introduced with the vector. After the selection, most of the cells expressed transgenes. To express Cldn3 in HPPL-Rab25 and HPPL-Cldn4 or dnRab25 in HPPL-Grhl2, we inserted

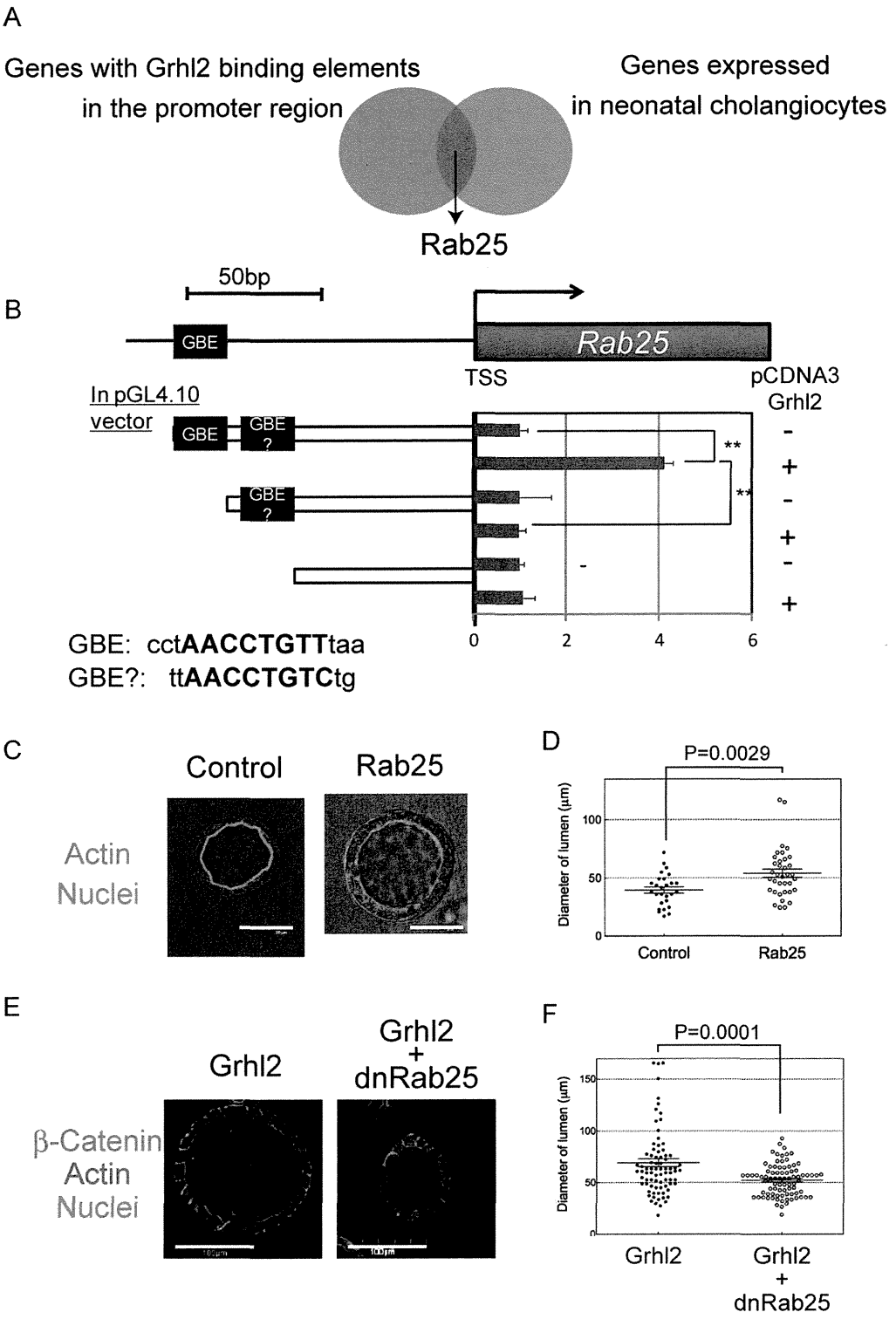

FIGURE 5: The small GTPase Rab25, a target of Grhl2, is involved in the enlargement of a central lumen induced by Grhl2. (A) A schematic view for the identification of Rab25. The consensus DNA sequence for Grhl2 binding (AACCGGTT) was searched in the database for human and mouse genes. More than 1000 genes were found to contain the sequence within 1000 base pairs upstream of the transcription initiation site. Among those genes, Rab25 was selected as a Grhl2 target since it was up-regulated in P1 cholangiocytes (shown by the microarray result comparing neonatal cholangiocytes with hepatoblasts) and might be involved in the intracellular localization of Cldn4. (B) A potential Grhl2-binding site in the promoter region of Rab25 gene is necessary for up-regulation of Rab25 mRNA by Grhl2. Luciferase activity is detected in the presence of Grhl2, whereas the deletion of a possible binding site (GBE) diminishes the expression of luciferase. GBE, grhl2-binding element. (C, D) Overexpression of Rab25 induces the enlargement of a

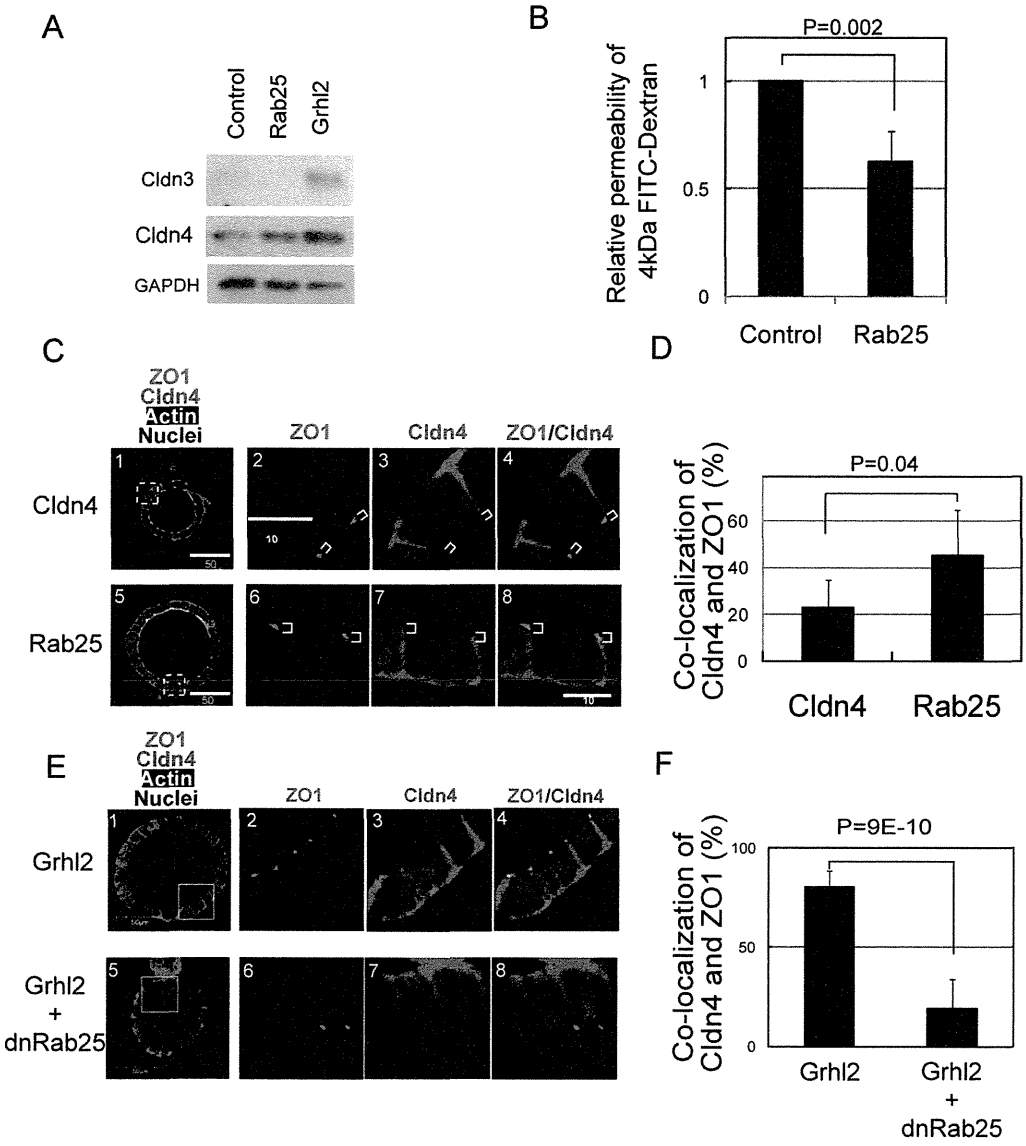

FIGURE 6: Rab25 increases Cldn4 protein and regulates its localization at TJs. (A) Rab25 increases the level of Cldn4 protein. Western blot data demonstrate that Rab25 increases Cldn4 protein but not Cldn3. (B) Rab25 enhances barrier function of the monolayer of HPPL. Rab25 decreases paracellular efflux of 4-kDa FITC-dextran, indicating that the barrier function of HPPL monolayer is enhanced. The control HPPL and HPPL-Rab25 were cultured on Transwells and used to examined the efflux of FITC-dextran. Experiment was repeated three times independently. (C, D) Rab25 promotes the localization of Cldn4 at TJs. Cldn4 (red) is barely colocalized with ZO1 (green) in HPPL-Cldn4 (C1–C4), whereas it is colocalized with ZO1 in HPPL-Rab25 (C5–C8). More than 50 lateral membranes derived from five cysts were analyzed for localization of Cldn4 and ZO1. The result is shown in D, indicating that Rab25 significantly increases colocalization of Cldn4 and ZO1. (E, F) dnRab25 inhibits the localization of Cldn4 at TJs. Cldn4 (red) is colocalized with ZO1 (green) in HPPL-Grhl2 (E1–E4), whereas it is not colocalized with ZO1 in HPPL-Grhl2+Rab25 (E5–E8). More than 100 lateral membranes derived from 10 cysts were analyzed for localization of Cldn4 and ZO1. The result is shown in F, indicating that dnRab25 significantly inhibits colocalization of Cldn4 and ZO1.

central lumen. (C) Representative cysts derived from HPPL and HPPL-Rab25. A cyst derived from HPPL-Rab25 has a central lumen surrounded by F-actin bundles (green) larger than the control HPPL. (D) Dot plot with bars of mean ± SEM for a representative culture, indicating that HPPL-Rab25 increased the size of lumen with statistical significance. HPPL and HPPL-Rab25 were cultured for 7 d, and the diameter of the central lumen was measured for >50 cysts per culture. Experiments were repeated four times independently. Bar, 50 μm. (E, F) Inhibition of Rab25 by a dominant-negative form of Rab25 in HPPL-Grhl2 resulted in decreased lumen size. (E) Representative cysts derived from HPPL-Grhl2 and HPPL-Grhl2+Rab25. Cysts derived from HPPL-Grhl2+dnRab25 have a central lumen smaller than HPPL-Grhl2. (F) Dot plot with bars of mean ± SEM for a representative culture, indicating that dnRab25 reduces the size of the central lumen with statistical significance. HPPL-Grhl2 and HPPL-Grhl2+dnRab25 were cultured for 7 d. The diameter of the lumen was measured >50 cysts per culture. Experiments were repeated for four times independently. Bars, 100 μm.

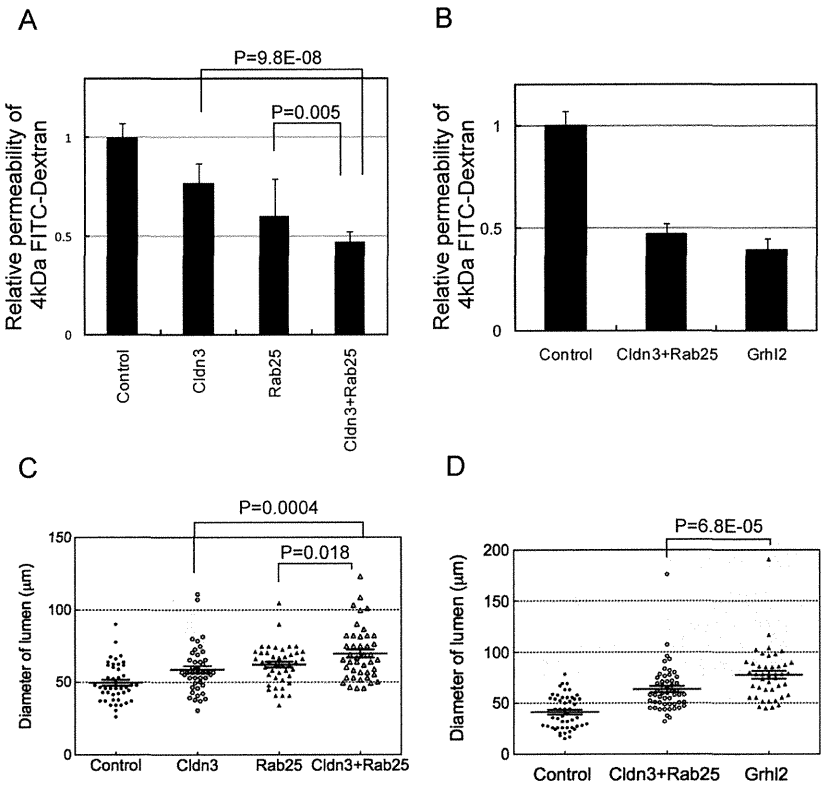

FIGURE 7: Cldn3 and Rab25 have additive effect on increasing barrier function and the lumen size. (A) HPPL-Cldn3+Rab25 shows stronger barrier function than HPPL-Cldn3 or HPPL-Rab25. Paracellular efflux of 4-kDa FITC-dextran is further decreased by coexpression of Cldn3 and Rab25 in HPPL as compared with expression of either of them. (B) HPPL-Cldn3+Rab25 and HPPL-Grhl2 show similar barrier function. (C) HPPL-Cldn3+Rab25 form significantly larger cysts than HPPL-Cldn3 or HPPL-Rab25. The size of lumen is further increased by coexpression of Cldn3 and Rab25 in HPPL as compared with expression of either of them. A dot plot for a representative culture is shown. The diameter of the lumen was measured for >50 cysts per culture. Experiment was repeated for three times independently. (D) HPPL-Grhl2 forms significantly larger cysts than HPPL-Cldn3+Rab25.

Cldn3 or dnRab25 cDNA into another retrovirus vector, pMXsPuro. After infection, HPPL were treated with 10 μg/ml puromycin. The promoter sequence of Rab25 containing 1000 base pairs upstream of the transcription initiation site was amplified from genomic DNA of embryonic kidney. It was inserted into pMD20. The proximal region was amplified and inserted into pGL4 vector.

Immunofluorescence chemistry

Fetal, neonatal, and adult livers were fixed in PBS containing 4% paraformaldehyde (PFA) and embedded in OCT compound. Thin sections were prepared with a microtome. For staining of Cldns in 2D culture of HPPL, samples were fixed in 1% PFA, permeabilized with 0.2% Triton-X100, and then incubated in Block Ace solution (DS Pharma Biomedical, Osaka, Japan). HPPL cultured in 3D conditions were treated as reported previously (Tanimizu *et al.*, 2007). Primary antibodies used for immunofluorescence were mouse anti–β-catenin (1:1500; BS Biosciences), rabbit anti-Cldn3 (1:500; Bioworld, Minneapolis, MN), rabbit anti-Cldn4 (1:500; a gift from Mikio Furuse, Kobe University, Kobe, Japan), rat anti-ZO1 (1:2000; a gift from Bruce Stevenson, University of Alberta, Edmonton, Canada), rat anti-EpCAM (1:500; BD Biosciences), rabbit anti-laminin (1:1000; Sigma-Aldrich, St. Louis, MO), and rabbit anti-Grhl2 (1:350; Sigma-Aldrich). Signals were visualized with Alexa Fluor–conjugated secondary antibodies (Molecular Probes, Eugene, OR) used at a dilution of 1:500. F-Actin bundles were detected with Alexa Fluor 488– or 633–conjugated phalloidin (Molecular Probes) at a dilution of 1:250. Nuclei were counterstained with Hoechst 34580. Samples were examined on Zeiss LSM 510 (Zeiss, Jena, Germany) and Olympus FV1000D IX81 (Olympus, Tokyo, Japan) confocal laser scanning fluorescence microscopes.

Live cell imaging

HPPL expressing yellow fluorescent protein–actin were kept in 5% Matrigel for 2.5 d in a two-well coverglass chamber (Nunc/Thermo Fisher Scientific, Rochester, NY) and then set onto the stage of an Olympus ID51 FV1000. The temperature and CO_2 concentration were kept at 37°C and 5%, respectively. Fifteen points were selected and followed for 32 h. Every 40 min, an *xy* image was captured at each point.

Measurement of transepithelial resistance and paracellular tracer flux

Aliquots of 2×10^5 cells were plated on a 12-mm Transwell with 0.4-μm-pore polyester membrane (Corning, Corning, NY). Transepithelial resistance (TER) was measured directly in culture medium using a Millicell-ERS epithelial volt-ohm meter (Millipore, Billerica, MA) at day 3 of the culture. The TER values were calculated by subtracting the background TER of blank filters, followed by multiplying by the surface area of the filter (1.12 cm^2). For the paracellular tracer flux assay, 4-kDa FITC-dextran (Sigma-Aldrich) was added to the medium inside the Transwell at day 3 at a concentration of 1 mg/ml. After incubation for 2 h, an aliquot of medium was collected from the basal compartment. The paracellular tracer flux was determined as the amount of FITC-dextran in the basal medium, which was measured with an Arvo SX fluorometer (PerkinElmer, Waltham, MA).

SDS–PAGE and immunoblotting

HPPL were cultured on a 12-mm Transwell, washed three times with ice-cold PBS, and then lysed in 150 μl of PBS containing 1% Triton-X as previously reported (Yoshii *et al.*, 2005). After scraping of cells into a microcentrifuge tube, they were placed on ice with several agitations, followed by centrifugation at 20,400 × *g* for 30 min. The supernatant was used as the Triton-X–soluble fraction. The pellet was added with 150 μl of PBS containing 0.1% SDS and then treated with an ultrasonicator. After centrifugation, the supernatant was transferred into a new tube and used as the Triton-X–insoluble fraction. Samples were separated by one-dimensional SDS–PAGE. For immunoblotting, proteins were electrophoretically transferred from gels onto Immobilon-P, a polyvinylidene difluoride membrane (Millipore). After incubation in Block Ace, the membrane was incubated with primary antibodies, including anti-Cldn2, 4, 6, and 8 (1:1000; gifts from Mikio Furuse), anti-Cldn3 (1:1000; Bioworld), anti-Cldn7 (1:1000; Abcam, Cambridge, MA), rabbit anti–cytokeratin 19 (CK19; 1:2000; Tanimizu *et al.*,

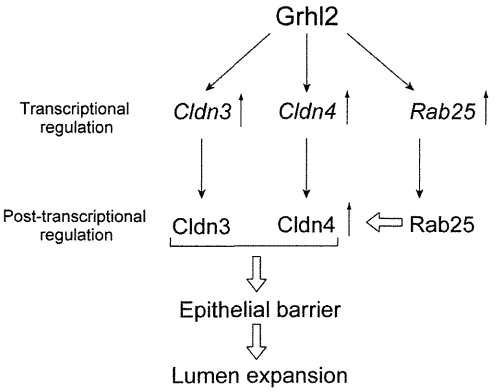

FIGURE 8: A molecular network governed by Grhl2 regulates the lumen size by modulating epithelial barrier function. Our results indicate that Grhl2 transcriptionally regulates Cldn3 and Cldn4, as well as Rab25, for enhancing epithelial morphogenesis, in particular, increasing the size of lumen. Cldns contribute to enhancing the barrier function of the HPPL monolayer, which is essential for the expansion of a central lumen of the cyst in 3D culture. Rab25 up-regulates Cldn4 protein and also promotes its localization at TJs, which induces lumen expansion.

2003), anti–glyceraldehyde-3-phosphate dehydrogenase (1:1000; Millipore). Bound antibodies were detected with horseradish peroxidase–conjugated secondary antibodies. SuperSignal West Dura Extended Duration Substrate (Pierce, Thermo Fisher Scientific, Rockford, IL) was used for the detection of peroxidase activity.

Culture with GST–C-CPE

pGEX6P-1 vector containing C-CPE and C-CPE313 were kindly provided by Mikio Furuse. GST proteins were purified using a glutathione–Sepharose 4B column (Amersham Pharmacia Biotech, Little Chalfont, United Kingdom) as previously reported. Eluted GST fusion proteins were dialyzed against PBS by using Amicon Ultracel-10K (Millipore). HPPL-Grhl2 were plated on the mixture of Matrigel and type I collagen (1:1, vol/vol) and covered with 5% Matrigel containing 100 μg/ml GST-C-CPE or GST-C-CPE313. Cells were kept at 37°C for 7 d.

Statistical analysis

The diameter of lumen was measured for >50 cysts in each culture. Culture was repeated at least three times. We confirmed that all the cultures for each set of HPPL transfectants gave similar results, and then we used a representative culture for each set of transfectants to show a dot plot in the figures. A *t* test was performed on Excel (Microsoft, Redmond, WA) to examine whether the diameter of a lumen was changed by expression of a gene of interest or by addition of peptides with statistical significance.

ACKNOWLEDGMENTS

We thank Mikio Furuse for providing us with antibodies against claudins and plasmid for expression of CPE peptides and for helpful discussions. We also thank Osamu Obara for providing us with cDNA of Grhl2. We appreciate the valuable technical assistance of Shigeru Saito and Eiko Saijo. We thank the members of the Miyajima and Mitaka laboratories for helpful discussions. This work was supported by a pilot grant from the University of California, San Francisco, Liver Center to N.T., National Institutes of Health Grants R01DK083330 and R01AI25144 to K.M., and research grants from the Ministry of Education, Culture, Sports, Science, and Technology, Japan, to N.T., A.M., and T.M.

REFERENCES

Antoniou A, Raynaud P, Cordi S, Zong Y, Tronche F, Stanger BZ, Jacquemin P, Pierreux CE, Clotman F, Lemaigre FP (2009). Intrahepatic bile ducts develop according to a new mode of tubulogenesis regulated by the transcription factor SOX9. Gastroenterology 136, 2325–2333.

Bagnat M, Cheung ID, Mostov KE, Stainier DY (2007). Genetic control of single lumen formation in the zebrafish gut. Nat Cell Biol 9, 954–960.

Bryant DM, Datta A, Rodriguez-Fraticelli AE, Peranen J, Martin-Belmonte F, Mostov KE (2010). A molecular network for de novo generation of the apical surface and lumen. Nat Cell Biol 12, 1035–1045.

Bryant DM, Mostov KE (2008). From cells to organs: building polarized tissue. Nat Rev Mol Cell Biol 9, 887–901.

Casanova JE, Wang X, Kumar R, Bhartur SG, Navarre J, Woodrum JE, Altschuler Y, Ray GS, Goldenring JR (1999). Association of Rab25 and Rab11a with the apical recycling system of polarized Madin-Darby canine kidney cells. Mol Biol Cell 10, 47–61.

Cheung ID, Bagnat M, Ma TP, Datta A, Evason K, Moore JC, Lawson ND, Mostov KE, Moens CB, Stainier DY (2011). Regulation of intrahepatic biliary duct morphogenesis by Claudin 15-like b. Dev Biol 361, 68–78.

Fitz JG (2002). Regulation of cholangiocyte secretion. Semin Liver Dis 22, 241–249.

Goldenring JR, Shen KR, Vaughan HD, Modlin IM (1993). Identification of a small GTP-binding protein, Rab25, expressed in the gastrointestinal mucosa, kidney, and lung. J Biol Chem 268, 18419–18422.

Gray RS, Cheung KJ, Ewald AJ (2010). Cellular mechanisms regulating epithelial morphogenesis and cancer invasion. Curr Opin Cell Biol 22, 640–650.

Lemaigre FP (2003). Development of the biliary tract. Mech Dev 120, 81–87.

Martin-Belmonte F, Mostov K (2008). Regulation of cell polarity during epithelial morphogenesis. Curr Opin Cell Biol 20, 227–234.

Moriwaki K, Tsukita S, Furuse M (2007). Tight junctions containing claudin 4 and 6 are essential for blastocyst formation in preimplantation mouse embryos. Dev Biol 312, 509–522.

Nam KT *et al.* (2010). Loss of Rab25 promotes the development of intestinal neoplasia in mice and is associated with human colorectal adenocarcinomas. J Clin Invest 120, 840–849.

Okabe M, Tsukahara Y, Tanaka M, Suzuki K, Saito S, Kamiya Y, Tsujimura T, Nakamura K, Miyajima A (2009). Potential hepatic stem cells reside in EpCAM+ cells of normal and injured mouse liver. Development 136, 1951–1960.

Pyrgaki C, Liu A, Niswander L (2011). Grainyhead-like 2 regulates neural tube closure and adhesion molecule expression during neural fold fusion. Dev Biol 353, 38–49.

Tanimizu N, Miyajima A, Mostov KE (2007). Liver progenitor cells develop cholangiocyte-type epithelial polarity in three-dimensional culture. Mol Biol Cell 18, 1472–1479.

Tanimizu N, Nishikawa M, Saito H, Tsujimura T, Miyajima A (2003). Isolation of hepatoblasts based on the expression of Dlk/Pref-1. J Cell Sci 116, 1775–1786.

Tsukita S, Furuse M (2002). Claudin-based barrier in simple and stratified cellular sheets. Curr Opin Cell Biol 14, 531–536.

Tzaban S, Massol RH, Yen E, Hamman W, Frank SR, Lapierre LA, Hansen SH, Goldenring JR, Blumberg RS, Lencer WI (2009). The recycling and transcytotic pathways for IgG transport by FcRn are distinct and display an inherent polarity. J Cell Biol 185, 673–684.

Werth M *et al.* (2010). The transcription factor grainyhead-like 2 regulates the molecular composition of the epithelial apical junctional complex. Development 137, 3835–3845.

Wilanowski T *et al.* (2008). Perturbed desmosomal cadherin expression in grainy head-like 1-null mice. EMBO J 27, 886–897.

Yoshii T, Mizuno K, Hirose T, Nakajima A, Sekihara H, Ohno S (2005). sPAR-3, a splicing variant of PAR-3, shows cellular localization and an expression pattern different from that of PAR-3 during enterocyte polarization. Am J Physiol Gastrointest Liver Physiol 288, G564–G570.

Yu Z, Bhandari A, Mannik J, Pham T, Xu X, Andersen B (2008). Grainyhead-like factor Get1/Grhl3 regulates formation of the epidermal leading edge during eyelid closure. Dev Biol 319, 56–67.

Yu Z, Mannik J, Soto A, Lin KK, Andersen B (2009). The epidermal differentiation-associated Grainyhead gene Get1/Grhl3 also regulates urothelial differentiation. EMBO J 28, 1890–1903.

Zegers MM, O'Brien LE, Yu W, Datta A, Mostov KE (2003). Epithelial polarity and tubulogenesis in vitro. Trends Cell Biol 13, 169–176.

Zong Y, Panikkar A, Xu J, Antoniou A, Raynaud P, Lemaigre F, Stanger BZ (2009). Notch signaling controls liver development by regulating biliary differentiation. Development 136, 1727–1739.

Current Biology 22, 1166–1175, July 10, 2012 ©2012 Elsevier Ltd All rights reserved DOI 10.1016/j.cub.2012.05.016

Article

Hypertrophy and Unconventional Cell Division of Hepatocytes Underlie Liver Regeneration

Yuichiro Miyaoka,[1] Kazuki Ebato,[1] Hidenori Kato,[1] Satoko Arakawa,[2] Shigeomi Shimizu,[2] and Atsushi Miyajima[1,*]

[1]Laboratory of Cell Growth and Differentiation, Institute of Molecular and Cellular Biosciences, The University of Tokyo, Yayoi, Bunkyo-ku, Tokyo 113-0032, Japan

[2]Department of Pathological Cell Biology, Medical Research Institute, Tokyo Medical and Dental University, Yushima, Bunkyo-ku, Tokyo 113-8510, Japan

Summary

Background: The size of organs and tissues is basically determined by the number and size of their cells. However, little attention has been paid to this fundamental concept. The liver has a remarkable ability to regenerate after surgical resection (partial hepatectomy [PHx]), and hepatocytes account for about 80% of liver weight, so we investigate how the number and size of hepatocytes contribute to liver regeneration in mice. It has been generally accepted that hepatocytes undergo one or two rounds of cell division after 70% PHx. However, ploidy of hepatocytes is known to increase during regeneration, suggesting an unconventional cell cycle. We therefore examine cell cycle of hepatocytes in detail.

Results: By developing a method for genetic fate mapping and a high-throughput imaging system of individual hepatocytes, we show that cellular hypertrophy makes the first contribution to liver regeneration; i.e., regeneration after 30% PHx is achieved solely by hypertrophy without cell division, and hypertrophy precedes proliferation after 70% PHx. Proliferation and hypertrophy almost equally contribute to regeneration after 70% PHx. Furthermore, although most hepatocytes enter cell cycle after 70% PHx, not all hepatocytes undergo cell division. In addition, binuclear hepatocytes undergo reductive divisions to generate two mononuclear daughter hepatocytes in some cases.

Conclusions: Our findings demonstrate the importance of hypertrophy and the unconventional cell division cycle of hepatocytes in regeneration, prompting a significant revision of the generally accepted model of liver regeneration.

Introduction

How the size of organs and tissues is regulated in development and regeneration is a fundamental question in biology [1, 2]. Fankhauser's historical observation of salamanders with a different ploidy demonstrated that cell numbers are inversely correlated with cell size and ploidy, allowing the organ size to remain the same [3]. A similar observation was made in tetraploid mouse embryos [4]. In the *Drosophila* wing, cells undergo atrophy/hypertrophy to compensate for changes in cell number to maintain the size of imaginal discs [5]. Furthermore, it has been demonstrated that the difference in the size of an organ in various mammals is mainly due to cell number, not cell size [6]. These are a few examples of studies showing the relation between organ size and the number and size of cells comprising the organ. However, not much attention has been paid to how cell size and number contribute to organ size in development and regeneration.

The liver has a remarkable capacity to regenerate. Even when 70% of its mass is surgically removed, the remnant tissue expands to compensate for the lost tissue and functions [7, 8]. The multilobular structure of rodent livers allows the surgical resection of a lobe of choice to achieve different levels of loss of liver mass by partial hepatectomy (PHx). Because the resection of lobes does not induce damage to the remaining tissue, PHx is a clean model. Therefore, liver regeneration after PHx has long been an excellent experimental model for tissue regeneration. Furthermore, although the liver consists of various types of cells, hepatocytes account for about 80% of liver weight and about 70% of all liver cells [9]. Thus, hepatocytes provide an ideal model to study the relation of organ size with number and size of cells.

It has been generally accepted that liver regeneration depends mainly on the proliferation of hepatocytes [7, 8, 10, 11]. In the simplest model without considering the possible change of cell size, all hepatocytes are expected to divide about 1.6 times after 70% PHx. However, there are several reports showing hypertrophy of hepatocytes in the regenerated liver [12–14] and it has not been investigated how the proliferation and hypertrophy of hepatocytes contribute to liver regeneration. Previous studies using the uptake of tritiated-thymidine showed that at least 84% of hepatocytes enter into S phase during liver regeneration [15]. However, entry into S phase does not necessarily mean cell division. Moreover, it is known that the ploidy of hepatocytes increases in the regenerated liver, suggesting that S phase is not always followed by a normal M phase [14, 16]. In addition, adult liver has many binuclear hepatocytes and the number of binuclear hepatocytes decreases during the regeneration [17]. These observations suggest that the cell division cycle of hepatocytes in regenerating liver may not follow normal processes. However, conventional analyses using bulk hepatocytes do not provide sufficient information as to the mechanism underlying such unique features of hepatocyte proliferation during regeneration.

To revisit the fundamental questions on the contribution of the size and number of hepatocytes to regeneration after PHx, we have developed two novel systems. One is an unbiased high-throughput system using an imaging cytometer to evaluate cell and nuclear size, number of nuclei, and expression of cell cycle markers in a large number of hepatocytes at the same time. The other is a genetic tracing system that marks individual cells permanently and randomly using transient expression of Cre recombinase by hydrodynamic tail vein injection (HTVi) [18], which allows the evaluation of cell division at the single-cell level. The imaging cytometric analysis revealed that the size of hepatocytes increases significantly, and hypertrophy and proliferation almost equally contribute to the regeneration after 70% PHx. Regeneration after 30% PHx and the initial phase of the regenerative process after 70% PHx depend solely on hypertrophy but not proliferation. Surprisingly, genetic tracing experiments showed that

*Correspondence: miyajima@iam.u-tokyo.ac.jp

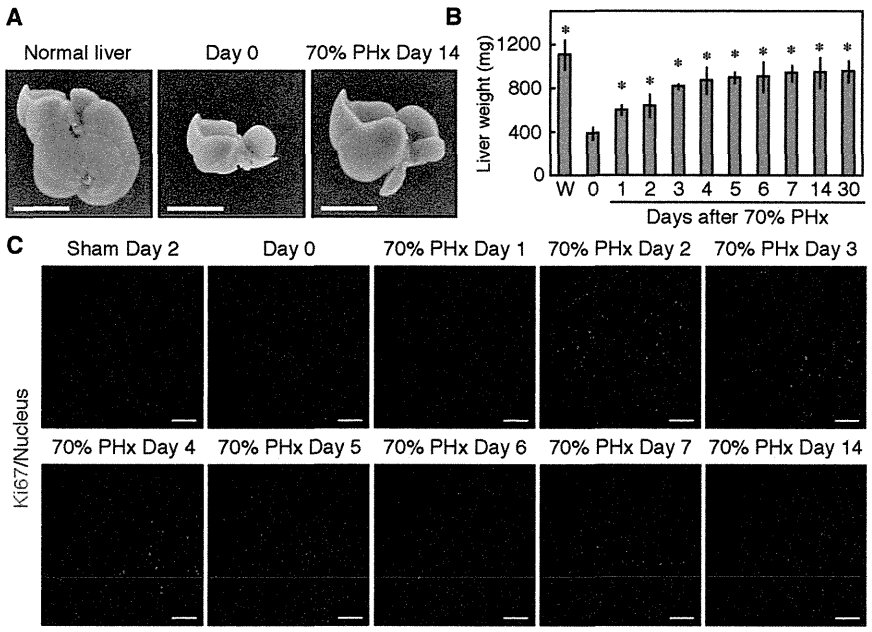

Figure 1. Liver Regeneration after 70% PHx

(A) Liver regeneration. The median and left lobes were surgically removed in 70% PHx. The remaining tissue expanded in mass by 14 days after 70% PHx. Scale bars represent 1 cm.

(B) Changes of liver weight during liver regeneration. p value between each time point and day 0 was calculated by Student's t test (*$p < 0.001$). Error bars represent SD. W, whole liver before PHx.

(C) Time course of entry into cell cycle of hepatocytes during liver regeneration. Immunofluorescent staining of Ki67 (red) was performed on liver sections at each time point after 70% PHx. Nuclei (blue) were stained with Hoechst33342. Note that at 1 day after 70% PHx, very few cells were $Ki67^+$, whereas the liver weight significantly increased. Quantification of $Ki67^+$ hepatocytes is shown in Figure S5E. Scale bars represent 100 μm.

only about half of hepatocytes undergo cell division during regeneration after 70% PHx. Moreover, we found that binuclear hepatocytes undergo reductive cell divisions to generate two mononuclear daughter hepatocytes and revealed unconventional cell cycle progression of hepatocytes during liver regeneration. In this paper, we provide various lines of evidence showing unique features of hepatocytes in regeneration, which require a significant revision of the generally accepted view of liver regeneration.

Results

Liver Weight Increases without Proliferation of Hepatocytes at the Early Phase of Liver Regeneration

In mice, liver weight increased from 1 day after 70% PHx and reached a plateau by 7 days as reported previously (Figures 1A and 1B) [7]. The remaining liver lobes increased about 2.4-fold in weight during the regeneration (Figure 1B). TUNEL assays showed no obvious apoptosis throughout the regenerative processes (Figure S1 available online) as shown previously [19], excluding the effects of apoptosis on the number of hepatocytes. Immunofluorescent staining of Ki67, which is expressed from the G1 to M phase but not in the G0 phase, clearly showed that hepatocytes vigorously entered the cell cycle at 2 days after 70% PHx, but the number of $Ki67^+$ cells dropped at 3 days after 70% PHx (Figure 1C). We quantified the proportion of $Ki67^+$ hepatocytes and found that it was less than 1% and about 49% at 1 and 2 days after 70% PHx, respectively (see below and Figures S5B and S5E). Interestingly, although there were few $Ki67^+$ hepatocytes at 1 day after 70% PHx, liver weight had increased considerably by that time (Figures 1B and 1C). These results indicated that the proliferation of hepatocytes alone could not account for the recovery of liver mass after 70% PHx. Therefore, we investigated the size of hepatocytes during liver regeneration.

Hepatocytes Enlarge during Liver Regeneration

To investigate the size of hepatocytes, we developed a new imaging cytometric approach. Because hepatocytes are epithelial cells, their outlines can be visualized by actin staining (Figure 2A). The cytometer recognizes nuclei with a certain roundness at first and then the surrounding actin signals as the outline of a cell, allowing an estimation of cell size. Because hepatocytes are much larger than other cell types, they can be distinguished based on size. This procedure also recognizes both mononuclear and binuclear hepatocytes (Figure 2A) and allows us to scan a large number of hepatocytes in a liver section efficiently and thoroughly (Figure 2B). Then, we measured the area of each hepatocyte during liver regeneration and found an increase in size at 1 and 7 days after 70% PHx (Figure 2C). Quantitative analysis revealed that the size of hepatocytes had increased slightly as early as 3 hr after 70% PHx, peaked at 1 day after 70% PHx, and then gradually decreased (Figure 2D). Because the hepatocytes were significantly larger at 14 days after 70% PHx than the sham operation control, hypertrophy of hepatocytes was maintained even after the recovery of liver weight (Figure 2D). Although this tendency was maintained even at 30 days after 70% PHx, it was not statistically significant (Figure 2D). Therefore, we performed most experiments within 14 days after 70% PHx hereafter. We also found that the nuclei enlarged during regeneration, suggesting increased DNA content per nucleus (Figures 2C and 2E). However, nuclear hypertrophy does not seem to be a direct cause of cellular hypertrophy, because cellular hypertrophy precedes it (Figures 2C–2E). We converted the data on area and concluded that hepatocytes increased in volume by 2.0-fold and 1.5-fold at 1 and 14 days after 70% PHx, respectively (Figure 2F). These results provide quantitative evidence, for the first time, that not only the proliferation but also the hypertrophy of hepatocytes significantly contributes to liver regeneration. Notably, the early phase of liver regeneration is largely dependent on the hypertrophy of hepatocytes, because the increase in liver weight 1 day after 70% PHx matched the increase in hepatocyte size (Figures 1B and 2F). It is known that lipids accumulate in hepatocytes immediately after 70% PHx [20]. Consistently, oil-red O staining and electron microscopy revealed intensive lipid accumulation 1 day after 70% PHx (Figures S2A and S2B). However, these lipids disappeared by 14 days after 70% PHx (Figure S2B), indicating that the lipids accounted for, at least in part, the rapid increase in hepatocyte size after 70% PHx,

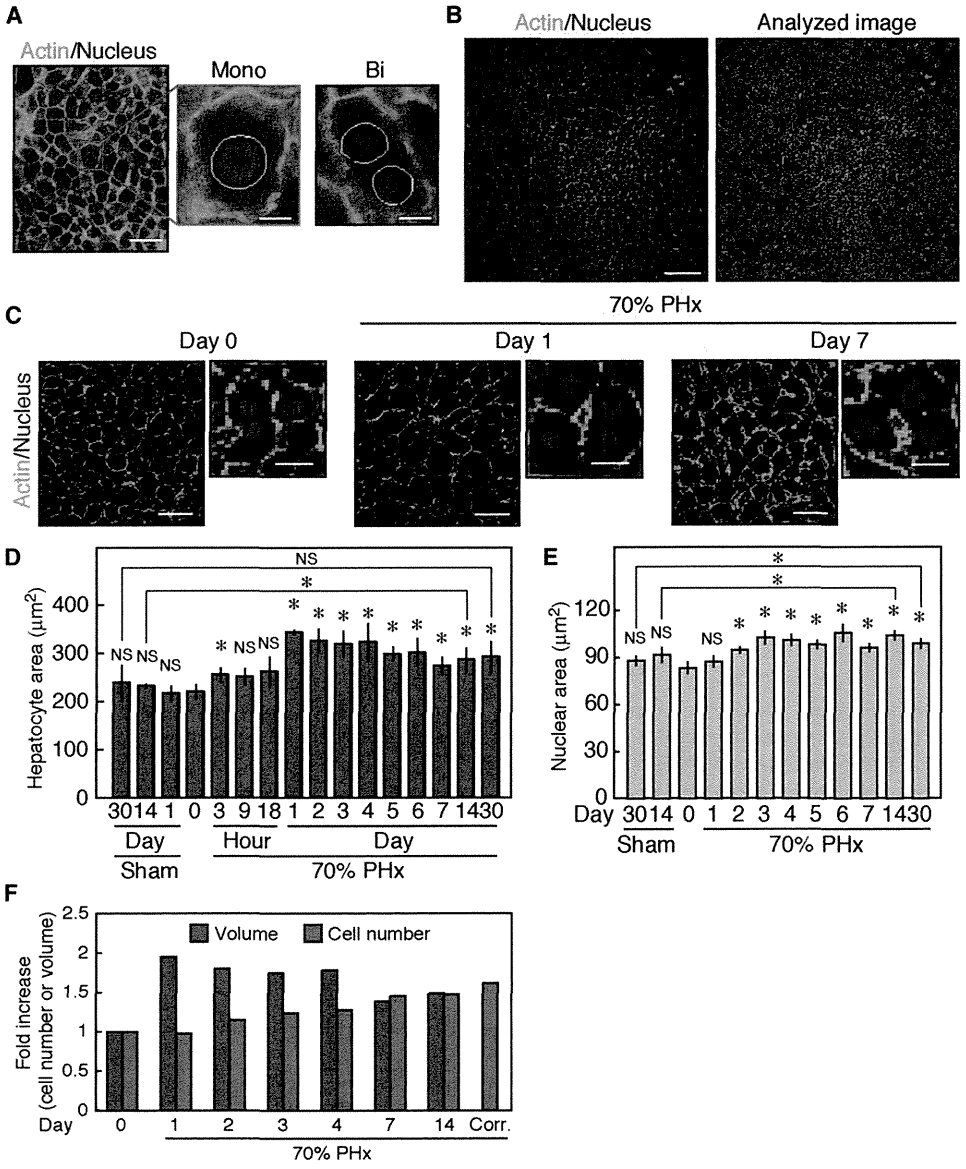

Figure 2. Hypertrophy of Hepatocytes during Liver Regeneration

(A) Recognition of nuclei and outlines of hepatocytes by imaging cytometry. Nuclei (blue) and actin (green) of hepatocytes were stained by Hoechst33342 and Phalloidin, respectively, in liver sections. The cytometer recognized nuclei (yellow) and outlines (magenta) of hepatocytes to calculate sectional area. This procedure also distinguishes mononuclear hepatocytes (Mono) from binuclear hepatocytes (Bi) and calculates their sectional area. Scale bars represent 25 μm for the left picture and 5 μm for the central and right pictures.

(B) An example of the analysis of liver sections by imaging cytometry. Actin (green) and nuclei (blue) staining allowed for the recognition of hepatocytes in liver sections. Scale bar represents 100 μm.

(C) The size of hepatocytes and their nuclei before and after 70% PHx. Actin (green) and nuclei (blue) staining showed hypertrophy of hepatocytes and their nuclei after 70% PHx. Note that hepatocytes increased their size whereas their nuclear size was not changed at day 1. Scale bars represent 25 μm for the larger photos and 12.5 μm for the smaller photos.

(D) Quantification of the size of hepatocytes during liver regeneration by imaging cytometry. The size of hepatocytes peaked at 1 day after 70% PHx and decreased thereafter. p values between each time point and day 0, and sham controls and the regenerated livers were calculated by Student's t test (*$p < 0.05$; NS, $p > 0.05$). Error bars represent SD.

(E) Quantification of the nuclear size of hepatocytes during regeneration after 70% PHx by imaging cytometry. The nuclear size increased after 70% PHx. p values between each time point and day 0, and sham controls and the regenerated livers were calculated by Student's t test (*$p < 0.01$; NS, $p > 0.05$). Error bars represent SD.

(F) Fold-increases in the volume and number of hepatocytes during liver regeneration. The values before PHx are set at 1. The volume was obtained by converting the sectional area of hepatocytes shown in (D), and the number was calculated from the quantified data on the labeled clusters of hepatocytes shown in Figure 3F. The fold-increase in the cell number 14 days after 70% PHx was corrected by the data obtained by serial section analysis (Figures 3G and 3H) and is also shown (Corr.). In the early phase, the liver regenerates almost entirely via hypertrophy. In the late phase, both hypertrophy and proliferation contribute to the regeneration.

but not the long-term hypertrophy. Furthermore, there was no remarkable change in organelles of hepatocytes in the regenerated liver (Figure S2B). Therefore, the density of hepatocytes before and after 70% PHx appears to be similar and the increase in liver weight is likely to reflect the increase in cell size.

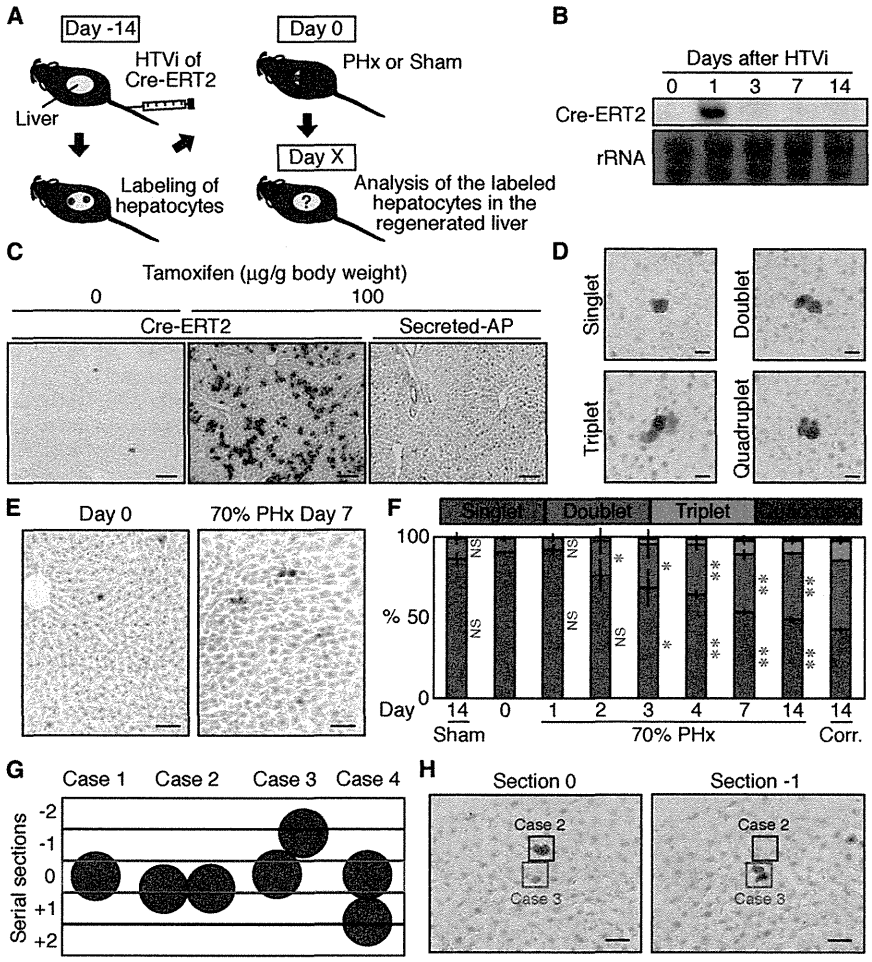

Figure 3. Genetic Labeling of Single Hepatocytes to Trace Cell Division

(A) Experimental scheme. The Cre-ERT2 expression vector was introduced into R26R mice by HTVi and DNA recombination was induced in hepatocytes. LacZ staining detected those hepatocytes that had undergone recombination. These mice were subjected to PHx or sham operation 14 days after HTVi and the $LacZ^+$ hepatocytes were analyzed in the regenerated liver at various time points.

(B) Northern blot analysis of expression of Cre-ERT2 after HTVi. rRNA was used as the loading control.

(C) Genetic labeling of hepatocytes. LacZ staining of liver sections 14 days after HTVi showed that administration of tamoxifen 3 days after HTVi of the Cre-ERT2 expression vector induced DNA recombination at a high frequency. DNA recombination did not occur at all on expression of secreted alkaline phosphatase (Secreted-AP) even in the presence of tamoxifen. Without tamoxifen, expression of Cre-ERT2 resulted in DNA recombination in a few hepatocytes. Scale bars represent 100 μm.

(D) Neighboring labeled hepatocytes observed in the regenerated liver. We defined clusters comprising one, two, three, and four $LacZ^+$ hepatocytes as singlets, doublets, triplets, and quadruplets, respectively. Scale bars represent 25 μm.

(E) LacZ staining of liver sections before and after 70% PHx. Before PHx (day 0), most labeled hepatocytes were singlets, whereas many doublets were observed 7 days after 70% PHx. Scale bars represent 50 μm.

(F) Quantification of the labeled clusters. Doublets increased from 2 days after 70% PHx. At 14 days after 70% PHx, about half of hepatocytes remained singlets. p values between each time point and day 0 for proportions of singlet (blue) and doublet (red) were calculated by Student's t test (*$p < 0.05$; **$p < 0.0005$; NS, $p > 0.05$). Those p values between the regenerated liver and the sham control at day 14 were also statistically significant ($p < 0.0005$) though not indicated. The data at day 14 corrected by the serial section analysis are also shown (Corr.) Error bars represent SD.

(G) Schematic representation of the serial section analysis. We first observed and counted the number of the labeled clusters of hepatocytes on one section (colored by red and designated as 0). Then, we observed additional two serial sections both above and underneath the first section (designated as −2, −1, +1, and +2). In case 1 and case 2, we could correctly detect singlets and doublets at position 0, whereas it is difficult to distinguish between singlets and doublets aligning in z dimension like case 3 and case 4. However, in case 3, singlets and doublets can be distinguished by comparing at position 0 and −1. Because the diameter of hepatocytes is 20–30 μm and the thickness of the sections was 20 μm, the additional four sections were enough to determine the fraction of overlooked cells. Although this serial section analysis may not distinguish neighboring hepatocytes aligned completely vertically to the first sections, this case must be very rare (case 4).

(H) Examples of the serial section analysis. Examples of case 2 (blue square) and case 3 (red square) are shown. An apparent singlet on a section at 0 position was revealed to be a doublet on a section at −1 position in case 3. Scale bars represent 50 μm.

Genetic Single-Cell Labeling Shows Less than One Cell Division of Hepatocytes on Average during Liver Regeneration

To directly evaluate cell division, we developed a new procedure to genetically label a single hepatocyte using hydrodynamic tail vein injection (HTVi), an efficient means of delivering genes to hepatocytes [18]. We introduced the Cre-ERT2 vector by HTVi into Rosa26-LacZ reporter (R26R) mice to genetically label hepatocytes (Figure 3A). Northern blot analysis showed that Cre-ERT2 was strongly expressed just after HTVi, but the expression dropped markedly thereafter (Figure 3B). At 14 days after HTVi, the expression of Cre-ERT2 was no longer detected (Figure 3B), but a large number of hepatocytes expressed LacZ when tamoxifen was administered at 3 days after HTVi of Cre-ERT2 (Figure 3C). By contrast, HTVi of secreted alkaline phosphatase as a control induced no recombination even in the presence of tamoxifen (Figure 3C). Unexpectedly, we noticed that HTVi of Cre-ERT2 did induce recombination even without tamoxifen in a few hepatocytes (Figure 3C). This tamoxifen-independent recombination was probably because of the strong transient expression of Cre-ERT2 in a few cells (Figure 3B). To trace each labeled cell, we utilized this low-frequency labeling without tamoxifen and performed PHx or a sham operation 14 days after HTVi, because the expression of Cre-ERT2 had vanished by that time (Figure 3B). There was no difference in liver regeneration between mice with and without HTVi, indicating that the liver had recovered from the damages, if any, caused by HTVi. Because hepatocytes exhibit different characteristics depending on the location in the liver lobule [21], we examined the location of the labeled hepatocytes and found that the genetic labeling occurred randomly throughout the lobule

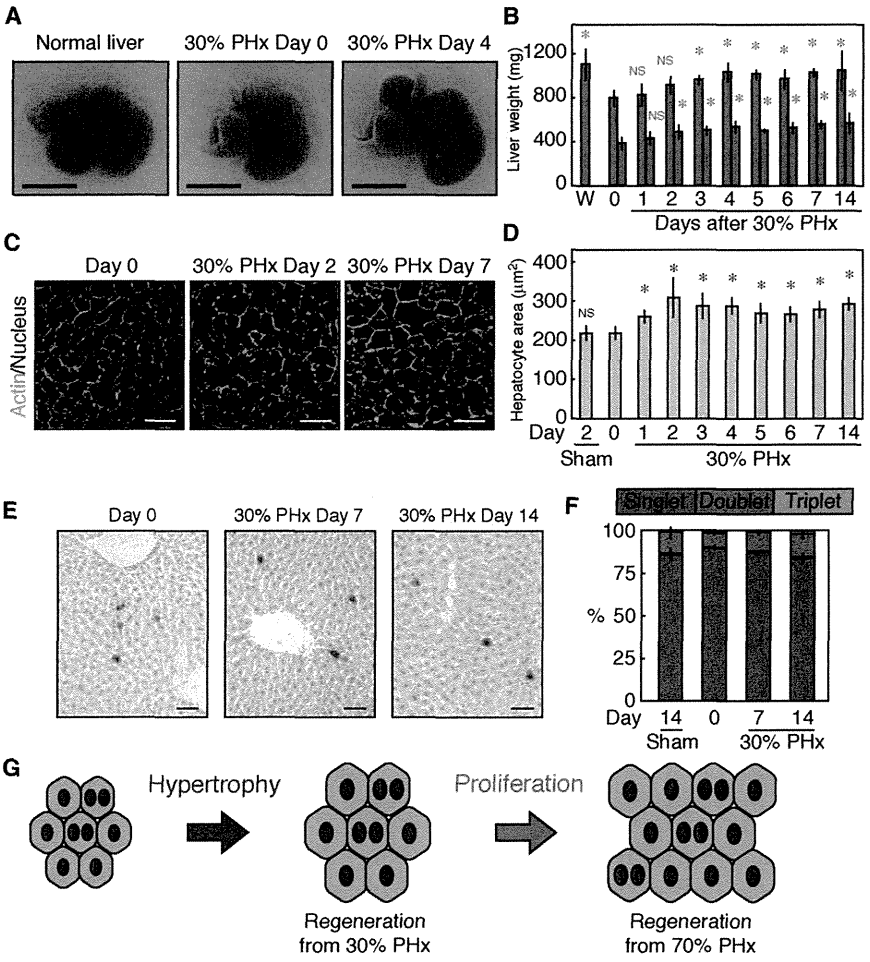

Figure 4. Cellular Hypertrophy and Cell Division of Hepatocytes after 30% PHx

(A) 30% PHx. In 30% PHx, the median lobe was surgically removed. The remaining lobes expanded by 4 days after 30% PHx. Scale bars represent 1 cm.

(B) Liver weight at different time points after 30% PHx. Because we analyzed right and caudate lobes in 70% PHx, we also analyzed them in 30% PHx. Thus, we separately weighed different lobes. Blue bars show weights of liver as a whole including all left, right, and caudate lobes, whereas red bars show those of only right and caudate lobes. p value between each time point and day 0 was calculated by Student's t test (*$p < 0.05$; NS, $p > 0.1$). Error bars represent SD.

(C) Images of hepatocytes after 30% PHx. Staining of actin (green) and nuclei (blue) showed that hepatocytes enlarged at 2 and 7 days after 30% PHx. Scale bars represent 25 μm.

(D) Quantification of the size of hepatocytes during liver regeneration after 30% PHx by imaging cytometry. p value between each time point and day 0 was calculated by Student's t test (*$p < 0.05$; NS, $p > 0.9$). Error bars represent SD.

(E) LacZ staining of hepatocytes after 30% PHx in the hepatocyte-labeling assay. Most of the LacZ$^+$ hepatocytes observed after 30% PHx remained as singlets. Scale bars represent 50 μm.

(F) Quantification of the labeled clusters. Proportions of singlet and doublet were almost the same between the regenerated liver at day 14 and the sham control ($p > 0.4$ by Student's t test), indicating that hepatocytes rarely underwent cell division after 30% PHx. Error bars represent SD.

(G) A model of liver regeneration. In the first response to the loss of liver mass, hepatocytes enlarge, which is sufficient for the loss of 30% mass. In the case of 70% PHx, hypertrophy is not sufficient, and hepatocytes proliferate to increase the cell number.

(Figure S3). We performed 70% PHx on these mice with the labeled hepatocytes and found clusters comprising various numbers of the labeled cells. We defined clusters of one, two, three, and four hepatocytes as singlets, doublets, triplets, and quadruplets, respectively (Figure 3D). Clusters comprising more than five hepatocytes were very rare in all the conditions examined (see below). If a singlet underwent one cell division during liver regeneration, it should become a doublet. Therefore, the cell division of individual hepatocytes during liver regeneration can be traced. We counted the numbers of labeled clusters at various time points during liver regeneration. Before PHx, most of the labeled hepatocytes were singlets, whereas a considerable number of doublets were observed at 7 days after 70% PHx (Figure 3E). Consistent with the Ki67 staining (Figure 1C), doublets started to significantly increase from 2 days after 70% PHx, and about a half of the labeled clusters were doublets at 14 days after PHx. Triplets and quadruplets also emerged, though their numbers were small. Interestingly, a considerable proportion of the labeled cells remained as singlets, suggesting that not all the hepatocytes undergo cell division during regeneration (Figure 3F). A possible problem of this analysis is, however, potential overlooking of neighboring hepatocytes aligned in z dimension, especially in regenerated livers where about half of the labeled cells had undergone cell division (Figure 3G). To address this possibility, we performed serial section analysis of the liver 14 days after 70% PHx. In addition to the section we first observed, we analyzed four additional serial sections to determine whether singlets in the first section are real singlets or doublets (Figures 3G and 3H). By this analysis, out of 93 apparent singlets, 9 turned out to be doublets and 3 were triplets, and out of 28 apparent doublets, 2 were triplets (Figure 3H and data not shown). With these values we corrected the data of 14 days after 70% PHx (Figure 3F). Even after the corrections, more than 42% of the labeled cells still remained as singlets. These results demonstrated that the number of hepatocytes increased by 1.6-fold during liver regeneration, which corresponded to an average of 0.7 cell division per cell (Figure 2F). As hepatocytes increased their volume by 1.5-fold (Figures 2D and 2F), the increases in the size and number of hepatocytes together ($1.5 \times 1.6 = 2.4$-fold) would account for the 2.4-fold increase in liver weight (Figure 1B). Our results provide the first quantitative data on the size and number of hepatocytes during liver regeneration and evidence that not only proliferation but also cellular hypertrophy roughly equally contributes to regeneration.

Liver Regenerates from 30% PHx by Hypertrophy of Hepatocytes without Proliferation

To address whether the proliferation and hypertrophy make similar contributions to all the regenerative processes, we next analyzed liver regeneration after 30% PHx (Figure 4A). Liver weight increased from 1 day after 30% PHx and reached a plateau by 4 days (Figures 4A and 4B). The right and caudate